Master's thesis

NTNU
Norwegian University of Science and Technology
Faculty of Natural Sciences
Department of Chemical Engineering

Solveig Stokka

Investigating Protein Adsorption on Hydrophobic and Hydrophilic Polymers for Antifouling Coatings

Master's thesis in Sustainable Chemical and Biochemical Engineering
Supervisor: Sulalit Bandyopadhyay and Angelika Brink
June 2023

NTNU
Norwegian University of Science and Technology

Solveig Stokka

Investigating Protein Adsorption on Hydrophobic and Hydrophilic Polymers for Antifouling Coatings

Master's thesis in Sustainable Chemical and Biochemical Engineering
Supervisor: Sulalit Bandyopadhyay and Angelika Brink
June 2023

Norwegian University of Science and Technology
Faculty of Natural Sciences
Department of Chemical Engineering

NTNU
Norwegian University of
Science and Technology

Abstract

Marine biofouling, settlement and growth of marine organisms on surfaces in seawater, has been a challenge since the oceans were first sailed. The process is typically initiated by adsorption of macromolecules such as proteins and polysaccharides, before diatoms, bacteria and larger organisms adsorb. Release of biocides has proven to be a highly effective antifouling method, but biocides are increasingly regulated and expected to phased out in the future. Extensive research has therefore been dedicated to develop effective, environmentally friendly antifouling coatings. One common approach based on surface wettability, where hydrophilic surfaces may resist adsorption and hydrophobic surfaces form week bonds with adsorbate, allowing for easy removal.

This thesis seeks to understand protein adsorption on surfaces with varying properties. Hydrophobic and hydrophilic surfaces with varying surface charge were obtained by forming self-assembled monolayers (SAMs) of polymers on gold sensors. Contact angle measurements were performed to study the wettability of the surfaces. The two proteins lysozyme and bovine serum albumin (BSA), and a binary mixture of the two, were dissolved in artificial seawater (ASW). They were then adsorbed on the polymeric SAMs using quartz crystal microbalance with dissipation (QCM-D), which allows for real-time detection of changes in mass and viscoelastic properties.

The results demonstrate significant differences in the adsorption kinetics between BSA and lysozyme. BSA exhibited rapid adsorption within a few minutes, whereas lysozyme displayed a slower adsorption process that continued for hours. The fast adsorption of BSA suggests a stronger affinity for the surface compared to lysozyme. In the mixed solution, BSA likely adsorbed as a monolayer, followed by the formation of a multilayer of lysozyme on top. This behavior is contrary to the conventional Vroman effect, where the protein with higher concentration displaces the protein with lower concentration from the surface. The observed behavior is likely a result of the high surface affinity exhibited by BSA.

The influence of ionic strength on protein adsorption processes appears to be of great significance. This phenomenon can be attributed to the formation of an electrical double layer of ions on charged and polar surfaces. Given the variation in salt concentrations across different geographic areas, comprehending the impact of ionic strength on adsorption becomes crucial. Understanding how changing salt concentrations affect the adsorption behavior provides valuable insights into the interaction between proteins and surfaces in diverse environments.

Sammendrag

Når overflater befinner seg i sjøvann vil ulike organismer fra sjøen adsorberes på overflaten. Dette fenomenet kalles marin begroing, og har vært et problem i årtusener. Første trinn i prosessen er typisk adsorpsjon av makromolekyler som proteiner og polysakkarider. Videre vil bakterier, kiselalger og større organismer feste seg på overflaten. For å forhindre den uønskede prosessen har det blitt utviklet ulike malinger. Malinger som inneholder biocider har vist seg å være svært effektive, men de er tungt regulert og forventes å fases ut i fremtiden på grunn av giftige effekter. Av denne grunn trengs nye alternativer som er både effektive og miljøvennlige. En tilnærming for å oppnå dette er å utvikle hydrofobe eller hydrofile overflater, som enten forhindrer adsorpsjon eller danner svake bånd slik at adsorbatet enkelt kan fjernes.

Målet med denne oppgaven er å oppnå en bedre forståelse av hvordan proteiner adsorberes på overflater med ulike egenskaper. Monolag av hydrofobe og hydrofile polymerer ble dannet på sensorer med gulloverflate. Karakterisering ble gjort ved å måle kontaktvinkelen til vann på overflatene. De to proteinene lysozym og bovint serumalbumin (BSA), og en miks av de to, ble løst i kunstig sjøvann (ASW). Videre ble "Quartz crystal microbalance (QCM)" brukt til å studere proteinadsorpsjon på polymerene.

Resultatene viser tydelige forskjeller i adsorpsjonskinetikken til de to proteinene. BSA adsorbertes raskt på alle overflater, og prosessen var ferdig etter få minutter. Adsorpsjon av lysozym viste lavere hastighet, men prosessen varte i flere timer og total masse adsorbert var betydelig høyere enn for BSA. Disse tendensene antyder at BSA hadde høyere affinitet mot overflaten. I den miksede løsningen med begge proteiner adsorbertes sannsynligvis ett molekylært lag av BSA først, før flere lag lysozym adsorbertes oppå dette. Tendensene er motsatt av Vroman-effekten, som ofte brukes til å beskrive konkurransemessig adsorpsjon av proteiner. Dette skyldes sannsynligvis den høye affiniteten BSA har til overflaten.

Effekten av ionestyrke i løsningen ser ut til å ha stor betydning for adsorpsjonsprosessen. Dette skyldes sannsynligvis at ioner adsorberes på overflater på ladede og polare overflater. Ettersom saltkonsentrasjon og ionestyrke varierer i ulike geografiske områder, er dette en sentral parameter for marin begroing.

Preface

This master thesis was written during the spring of 2023 and concludes my MSc in Sustainable Chemical and Biochemical Engineering at the Norwegian University of Science and Technology (NTNU).

The lab work of this project was performed at laboratories of the Department of Chemical Engineering, Department of Mechanical and Industrial Engineering and the cleanroom facilities at NTNU NanoLab.

The project was performed under the supervision team of Prof. Sulalit Bandyopadhyay (NTNU) and Prof. Angelika Brink (Jotun). I would like to express my biggest gratitude to my supervisors for providing insightful advice and information throughout the project. They have shown a huge working capacity and always been available when I have needed them despite hectic schedules. I am grateful that they gave me the opportunity to work on such a relevant and important topic.

I would also like to thank Hamid Khanmohammadi and Mathilde Isabelle Barriet for giving me instrument trainings. Thanks to Mathilde Isabelle Barriet and Jens Norrman for extremely valuable theoretical input and discussions.

I want to thank members of the Particle Engineering and Hydrometallurgy Research Team for sharing knowledge, helpful discussions, suggestions and support in team meetings.

Lastly, I would like to express my gratitude toward my parents. They have guided me in the right direction and always been my biggest motivators and cheerleaders.

Contents

List of Figures

List of Tables

Acronyms and Abbreviations

TBT	Tributyltin
EPS	Extracellular polymeric substances
MIC	Microbically influenced corrosion
PEG	Poly(ethylene glycol)
PDMS	Poly(dimethylsiloxane)
PDMSe	Poly(dimethylsiloxane) elastomers
SAM	Self-assembled monolayer
pI	Isoelectric point
BET	Brunauer-Emmett-Teller
QCM	Quartz crystal microbalance
QCM-D	Quartz crystal microbalance with dissipation monitoring
BSA	Bovine serum albumin
Lys	Lysozyme
ASW	Artificial seawater
MUA	11-Mercaptoundecanoic acid
MUOH	11-Mercapto-1-undecanol
DT10	1-Decanethiol
AUT	11-Amino-1-undecanethiol, hydrochloride
SDS	Sodium dodecyl sulfate
DI	Deionized
SE	Spectroscopic ellipsometry
MP-SPR	Multi-parameter surface plasmon resonance
TLTM	Too low to measure
Rms	Root mean square

Introduction

The shipping industry plays a significant role in international trade, accounting for more than than 80% of global trade by volume. The economic dependence on the oceans is estimated to grow from US$1.5 trillion to more than US$3.0 trillion by 2030. [1;11] This increase highlights the expected increase in marine activity and infrastructure, and the need for solving challenges in the marine sector. [12] Marine biological fouling, or marine biofouling, is an undesirable process that occurs immediately after surfaces are submerged into seawater. The process includes adsorption of macromolecules such as proteins and polysaccharides, before bacteria and larger organisms adsorb. Biofouling affects multiple areas in marine industries. In the case of ships, fouling causes reduced speed and maneuverability. It also leads to increased fuel consumption, and consequently higher emissions and economic costs. [13] In addition to shipping, biofouling affects the aquaculture field, desalination plants and other sectors. [14;13]

Antifouling paints containing derivates of the biocide tributyltin (TBT) have been used to control biofouling the past 50 years. However, TBT has shown toxic effects on non-target organisms and was therefore banned in 2008. Copper is currently employed as an alternative, but due to environmental concerns biocides have become increasingly regulated and are expected to be phased out in the future. consequently, there is a demand for environmentally friendly antifouling coatings with high performance. [15]

To develop such coatings, Understanding how the physicochemical properties of surfaces influence the biofouling process is essential. [16] The understanding of protein adsorption phenomena has advanced over the past decades through research in the field, but there are still differing, and even contradictory, viewpoints among researchers. [17] Protein adsorption mechanisms are still far from being completely understood, as it is a complex process impacted by multiple factors. [18]

This thesis presents an approach to understand the effect of wettability on protein adsorption. Lysozyme, bovine serum albumin (BSA) and a mixture of both proteins will be adsorbed onto polymer surfaces with varying hydrophobicity/hydrophilicity and charge characteristics. Quartz crystal microbalance with dissipation monitoring (QCM-D) will enable real-time analysis of changes in mass and viscoelastic property during the adsorption process.

Two main objectives for the project are set;
i) Formation of well-ordered and reproducible self-assembled monolayers (SAMs) of thiolates with distinct properties on gold sensors.
ii) Investigation of protein adsorption on surfaces exhibiting variations in wettability and charge.

1 Theory and Literature Review

In this section, the biofouling process and related challenges will be further explained. Development of antifouling approaches over the years and today's approaches will be discussed. The main focus will be on hydrophilic and hydrophobic coatings. Protein behavior and adsorption processes will also be discussed.

1.1 Marine Biofouling

1.1.1 Background and Factors Affecting Marine Biofouling

Marine biofouling has been a major challenge in the shipping industry since ancient times, and has remained a challenge to this day.[14;19;1] The phenomena occurs when various organisms settle on marine man-made structures submerged in the sea.[20;14] The process is complex, and includes a wide variety of organisms which can be divided into micro- and macrofoulers. Microfoulers include viruses, bacteria, fungi, protozoa and microalgae, while barnacles, mussels, tubeworms, sponges and anemones are examples of macrofoulers.[20;12]

The fouling process is influenced by a multitude of factors. Physical-chemical characteristics of seawater, including pH, temperature, dissolved oxygen and organic matter content, exert a significant impact on the fouling process. Other factors include hydrodynamic conditions such as distance to shore, current velocity, wave exposure, ship speed and voyage factor. The biofouling growth rate generally increases with temperature, meaning less fouling is expected close to polar areas with lower temperatures ($<$5 °C).[20]

1.1.2 Challenges Related to Marine Biofouling

Severe economic and environmental problems are caused by marine biofouling.[1] The accumulation of organisms on surfaces may cause higher exhaust gas emissions, surface cleaning and maintenance costs and economic losses related to fuel consumption.[21] Biofouling may increase fuel consumption by up to 40% and decrease speed by up to 10%.[12] Increased fuel consumption due to biofouling also yields higher emissions of CO_2, NO_X and SO_X. Biofouling increases the frequency of dry-dock operations needed, where the hull is cleaned, paint removed and repainted.[1]

A major part of biofouling related problems is economic losses.[1] The US Navy in 1981 consumed 18 million barrels of fuels, whereof 3.3 million were attributed to biofouling losses. Biofouling may also pose a safety risk, as algae on structures and walkways produce a slippery coating.[19] In addition, it may pose a risk to marine ecosystems, as invasive or non-native species attached on ship hulls may be introduced to new areas.[21;15]

Marine biofouling does not only affect the shipping industry. Membranes in desalination plants or reverse osmosis for water purification are also affected by biofouling. These have to be frequently replaced, which adds to the cost of water.[14] It is also a major challenge in regards to maintain a long and efficient operational lifespan of marine installations and equipment in the marine renewable energy sector. Challenges include loss of structural integrity and performance due to increased weight and thickness.[20]

A biofouling challenge relevant in all marine industries is induced or accelerated corrosion on surfaces through anaerobic microorganisms.[19] This is referred to as microbiologically influenced corrosion (MIC), and may be further facilitated by macrofoulers. If the coating of marine structures is physically damaged by attached organisms, the corrosion process may be further accelerated.[20;22]

1.1.3 The Biofouling Process

As displayed in Figure 1.1, the process of marine biofouling is typically divided into four steps: [20;1;13]

(i) A biochemical conditioning film consisting of inorganic and organic macromolecules such as glycoproteins, polysaccharides, nucleic acids and humic acids is formed within seconds to hours of immersion. [20;15] Bacterial adhesion is promoted by the conditioning film, as at modifies the physicochemical surface properties and constitutes a nutrient source. [13]
(ii) The second step is primary film formation, and takes place within hours. Bacteria and diatoms are transported to the surface due to various factors including gravity, diffusion and Brownian movement. The surface adhesion is initially reversible, and they adsorb weakly through van der Waals, hydrophobic and/or electrostatic interactions. [13;15] The bacteria and diatoms then adsorb irreversibly by secretion of adhesive extracellular polymeric substances (EPS). [20;1] Co-occurrence of bacteria and diatoms may synergistically increase the production of EPS. [23] These microorganisms and EPS further facilitate settlement of macrofoulers, as more organisms may be trapped due to irregular microbial colonies [20;13]
(iii) Multi-cellular species including soft-foulers and hard-foulers colonize the surface within days to weeks. These form a microfilm, and attract further settlements as they grow and age. [20;1]
(iv) Within weeks to months, animal larvae such as mussels and barnacles adsorb on the surface. [1]

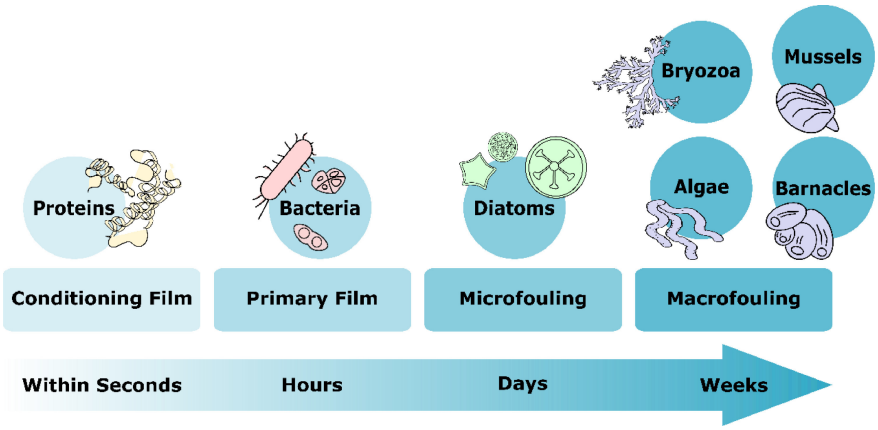

Figure 1.1: Schematic of the biofouling process with timelines. [1]

The four-step process described above is generally accepted by researchers and may represent patterns, but it is an oversimplification of the process and implies causality from stage to stage. [20;24] This is not necessarily the case, and it is possible that steps overlap or take place in parallel. [1] A more dynamic model is now widely accepted, where the absence of one stage does not inhibit other stages from occurring. [20]

This thesis is focused around understanding protein adsorption on relevant surfaces, and hence obtain a greater understanding of the mechanisms involved step 1. The rationale behind this approach is that by impeding step 1, subsequent steps can be minimized. Although a surface that resists protein adsorption may not necessarily resist all types of fouling organisms, it is highly likely to impede the settlement of numerous organisms due to the shared interactions involved in adsorption. Protein adsorption is also essential since fouling organisms frequently secrete adhesives composed of proteins and glycoproteins. [25]

1.2 Antifouling

1.2.1 Development of Antifouling Techniques

Various approaches have been explored for antifouling purposes since the earliest voyages across the oceans. Ancient seafarer nations like the Cartaginians and Phoenicans (1500-300 BC) are believed to have employed lead, pitch and copper plating for antifouling purposes. Use of wax, tar, asphalt, arsenic and sulfur has later been recorded. In the 18th century, copper sheathing emerged as an antifouling measure. However, its effectiveness diminished in the 19th century when iron-hulled ships came into general use. Copper-oxide-based paints were used on ship hulls from the mid-20th century. An issue related to these was rapid leaching, resulting in short life service and accumulation of copper salts in the environment.

A breakthrough occurred in 1960, when a self-polishing paint was developed. With this method, the antifouling inhibitor was stored in a polymer/copolymer matrix, which facilitated slow dissolution. The paint contained an organotin compound such as tributyltin (TBT) oxide.[19] TBT and related compounds were highly effective, and used on approximately 70% of the world fleet. These have later shown severe toxic impact on marine life, and were therefore banned worldwide in 2008.[19;12;15] In addition to TBT, other biocides such as zinc, zineb, pyridine, dichloroflumid and chlorothalonil have been employed.[26] Copper-based antifouling paints offering adequate protection against biofouling replaced TBT, and are still in use. Current commercial antifouling coatings are usually self-polishing copolymer paints with high levels of copper (40-75 wt%) and booster biocides.[15] However, copper concentrations >3.1 ppb affect various life stages of organisms and they are therefore thought to be environmentally unsafe.[12;27;15] All antifouling paints containing biocides are now facing strict regulations regarding release rate and registration processes.[1]

Increased attention is now drawn towards environmental aspects of biofouling.[1] Research in this field is growing rapidly, as there is an urgent need for development of environmentally friendly alternative coatings.[1] Lack of an ideal, cost-effective and environmentally friendly anti-fouling solution remains a great challenge for the marine industry.[12] In order to develop non-toxic antifouling coatings, a comprehensive understanding of how the physical and chemical characteristics of surfaces influence their tendencies to foul is crucial.[14]

Finding a universal antifouling coating has proven to be extremely difficult, as there is a huge variety in fouling species and adsorption mechanisms. Geographic location and seasonal changes also affect the biofouling process.[1;24] Surface treatment with an antifouling coating is currently the most successful and common antifouling method. The coatings should have a wide range of properties including high effectivity, long-term stability, durability, large-scale applicability and ecofriendliness.[28] Effective antifouling strategies must hinder primary adsorption (fouling-resistant) or permanently weaken adhesion (fouling-release).[1]

Figure 1.2 provides an overview of modern antifouling strategies. There are a wide variety of approaches, and several have shown promising results. This thesis focuses on antifouling coatings based on surface wettability, which is one of the most important surface parameters for development of new antifouling coatings.[1] Strategies of hydrophilic and hydrophobic coatings will be thoroughly discussed in the subsequent sections.

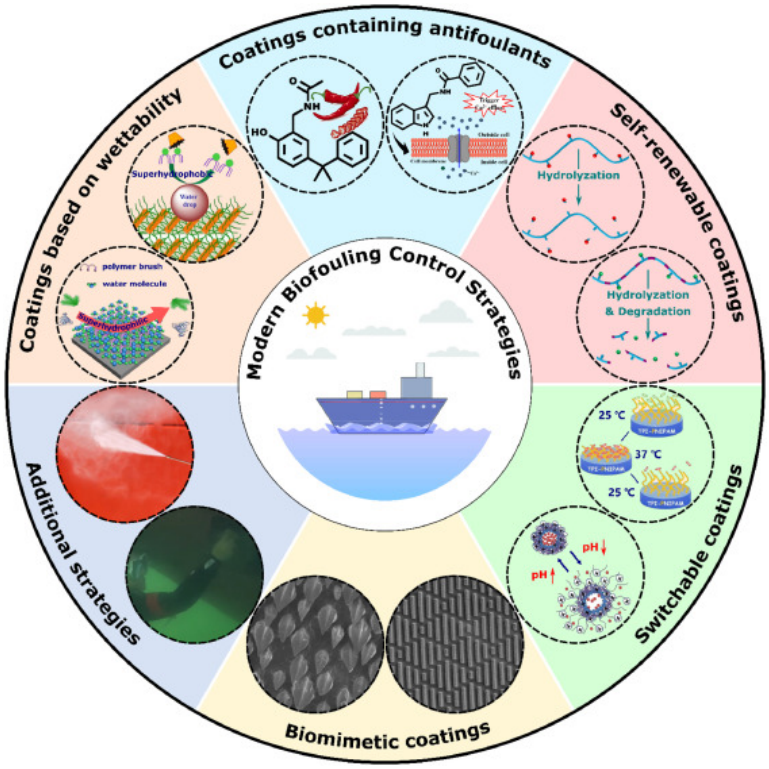

Figure 1.2: Illustration describing different modern antifouling approaches.[1]

1.2.2 Hydrophilic Coatings

Hydrophilic surfaces are surfaces that exhibit static water contact angles <90°, and surfaces exhibiting contact angle <300° are termed superhydrophilic.[29] They have gained significant attention for their antifouling properties in both marine and biomedical industries. Superhydrophilic surfaces possess surface energies similar to water (72 mN/m), and they tend to form a hydration layer on the surface. For these surfaces, it is thermodynamically favorable for the surface to remain in contact with water rather than other organisms. They therefore are a good antifouling option.[1;16]

Superhydrophilic coatings can be characterized as fouling-resistant coatings. The objective of such surfaces is hindering fouling organisms from attaching by modification of the surface chemistry.[24;28] Presence of charges on hydrophilic surfaces may facilitate or inhibit adsorption of marcromolecules and other organisms through electrostatic interactions.[25] By using electrically neutral polymers, potential electrostatic interactions between fouling organisms and surfaces can be avoided.[16] Settlement of marine organisms on synthetic neutrally charged hydrogels or hydrophilic polymers has proven to be very low both in laboratory and marine field tests.[25;30;31;32]

Charge neutrality has been recognized as an essential characteristic of protein-resistant self-assembled monolayers (SAMs). However, most surfaces will become charged after submersion in seawater due to adsorption of ions. Hence, it is also of considerable relevance to understand the effects of surface charge on fouling. The majority of materials and natural surfaces are negatively charged in aqueous solutions. Consequently, it is reasonable to expect that organisms have developed adsorption mechanisms adapted to anionic surfaces. Understanding the interplay between furface charge and fouling is thus highly relevant.[25]

One of the most successful polymers with good antifouling properties is poly(ethylene glycol) (PEG). Its chemical structure is presented in Figure 1.3. Low interfacial energy, non-toxicity,

high chain mobility and a hydration layer formed due to hydrogen bonds between ether oxygen atoms and water molecules are important characteristics. Electrical neutrality reduces electrostatic interactions between the polymer and biofoulants. PEG brushes have been given broad attention, as they are non-leaching and therefore environmentally friendly. [1;33] PEGylation, grafting PEG onto surfaces to develop PEG brushes, is still the standard strategy for inhibiting adsorption of numerous proteins. [28] However, PEG suffers from several drawbacks. Hydrolysis and biodegradation limit the long-term stability of the polymer. [1] PEG brushes have shown to lose their antifouling capacities when the temperature approaches 35℃, and oligo(ethylene glycol)-terminated SAMs decomposed after a month at 20℃. [33] Grafting PEG to chemically different surfaces also remains a challenge, since it often requires complex surface chemistry which can make scaling up expensive. [28] Various attempts have been made to improve the coating stability of PEG. [34;35;36]

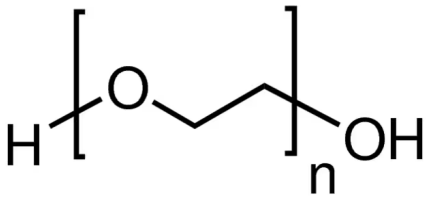

Figure 1.3: Chemical structure of the hydrophilic polymer PEG used for antifouling. [2]

Zwitterionic polymers have also shown promising antifouling performance, and they propose a good alternative for PEG. They are polymers with an equal positive and negative charge, i.e. polymers containing equal amounts of anionic and cationic groups in the molecular chain. A stronger hydration layer is formed on zwitterionic polymers than non-ionic polymers such as PEG, as they are subject to electrostatically induced hydration which renders them superhydrophilic. This electrostatically induced hydration caused by ions is stronger than the hydrogen bonding based interactions from ether groups in PEG. Hence, they are expected to exhibit better antifouling performance. [1;33] In addition to good antifouling performance, they are easy to functionalize and provide flexible design. Zwitterions can be classified into sulfobetaine (SB), carboxybetaine (CB) and phosphorylcholine (PC) depending on their anions, where anions are sulfonates, carboxylates and phosphonates for the three groups, respectively. Cations are typically quarternized ammonium. The most industrially relevant group is SB based polymers due to easy preparation. Some of these are commercially available. [33]

Hydrophilic polymers may also be fabricated as hydrogels. They exhibit good antifouling performance due to strong hydration ability and low elastic modulus. However, hydrogels suffer from short-term stability due to poor mechanical stability and adhesion to substrates, and their long-term applicability needs to be improved. [1]

1.2.3 Hydrophobic Coatings

Hydrophobic surfaces are characterized by having a water contact angle >90°, and surfaces exhibiting a water contact angle of >150° are superhydrophobic. There has been increased interest in developing hydrophobic coatings that exhibit fouling-release properties. The principle behind fouling-release coatings is that microorganisms adhere poorly to surfaces with low free energy. Hydrophobic surfaces only exhibit weak dispersive interactions with biomolecules. [1] The objective of fouling-release (FR) coatings is not to prevent foulants from attaching, but to create a weak interfacial bond to facilitate easy removal of attached organisms. This can be done by ships generating hydrodynamic shear forces, or by gentle grooming devices. [24;28] A disadvantage related to hydrophobic coatings is that the low surface free energy also causes low adhesion-to-substrate strength. The fouling-release effect can be enhanced by adding nano- or microscale roughness on the surface, leading to superhydrophobic behaviour. [1]

One class of hydrophobic coatings that has demonstrated excellent fouling-release properties

is polydimethylsiloxanes (Figure 1.4).[1;23] Commercial FR coatings are typically based on poly(dimethylsiloxane) elastomers (PDMSe). These polymers have low surface energy (∼22 mN/m) and hydrophobic character, and therefore propose reduced opportunities for hydrogen bonds and polar interactions. Another advantage of PDMSe is low elastic moduli. There are, however, some disadvantages related to PDMSe that limit their application. They are less durable and more easily damaged than other types of coatings, and their low surface energy makes them difficult to bond to substrates without an appropriate tie coat. The technology is also most effective on vessels with high voyage factors.[24] Antifouling properties of PDMSe frequently fails to diatoms.[33]Modification of PDMS has been subject to extensive research in attempts to reduce the disadvantages. This includes incorporation of additives and fabrication of copolymers and composites.[1] Several attempts have been made to improve the fouling control performance,[37;38;39;40] and to improve the mechanical stability and substrate adhesion.[41;42;43;44]

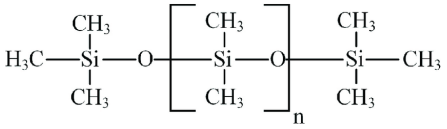

Figure 1.4: Chemical structure of the hydrophobic polymer PDMS used for antifouling.[3]

In addition to PDMS, fluoropolymers are used for hydrophobic antifouling coatings. These also form smooth, low-energy surfaces, but suffer from several drawbacks compared to PDMS. Lower elastic modulus requires higher shear force or critical stress. The fluorinated compounds may also be harmful to the environment due to high chemical and biological stability causing bioaccumulation. Another drawback is that they often lose their hydrophobicity and therefore fouling-release properties because of chain reorganization in water.[1]

1.2.4 Amphihpilic Coatings

Amphiphilic coatings are coatings containing both hydrophobic and hydrophilic groups.[23] Interest has increased in these over the past decade, and amphiphilic coatings are now considered one of the more promising antifouling strategies.[1;15] They have shown characteristics such as reduced biofilm formation and improved fouling-release properties on a wide range of organisms.[23]

Block copolymers are ideal for this purpose, as they guarantee nanometer sized hydrophobic and hydrophilic domains. Preparation is typically limited to the gram scale, and postmodification steps make it challenging to scale up the copolymer products for commercial use. Mixing block copolymers with thermoplastic elastomers or PDMS resins has recently demonstrated good antifouling performance. The functional groups of block copolymers typically migrate to the surface during processing, allowing for a copolymer concentration below 15 wt%.[28]

1.3 Protein Adsorption

1.3.1 Protein Characteristics

Protein adsorption processes are complicated, as proteins are molecules with complex compositions and molecular structures. It is crucial to understand the structure of protein molecules in order to understand the adsorption processes. Proteins typically consist of polypeptide chains with different amino acid sequences. These are linked together through hydrogen bonds, forming secondary structures such as α-helices and β-sheets. Further, tertiary structures are formed by interactions such as salt bridges, hydrogen bonds, disulfide bonds and electrostatic interactions. Due to the complexity of protein structure, the surface of a single protein may contain hydrophilic, hydrophobic, anionic and cationic regions simultaneously (Figure 1.5).[4;45]

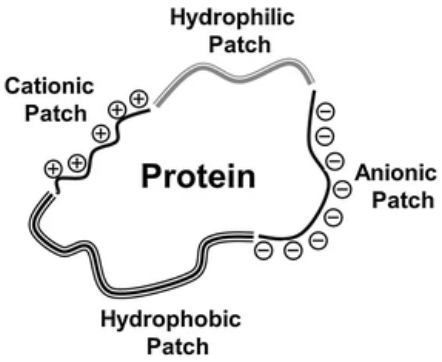

Figure 1.5: Schematic of the heterogeneous nature of protein surfaces. [4]

Environmental factors such as temperature, pH and ionic strength may influence distribution and proportion. [4] The complex structures of proteins enables interactions with charged, hydrophilic and hydrophobic molecules. They can also interact with each other and form protein complexes under favorable conditions. [46] The charge distribution, and therefore electrostatic interactions, are affected by the pH. The asymmetrical charge distribution of a lysozyme molecule under varying pH is illustrated in Figure 1.6. [5]

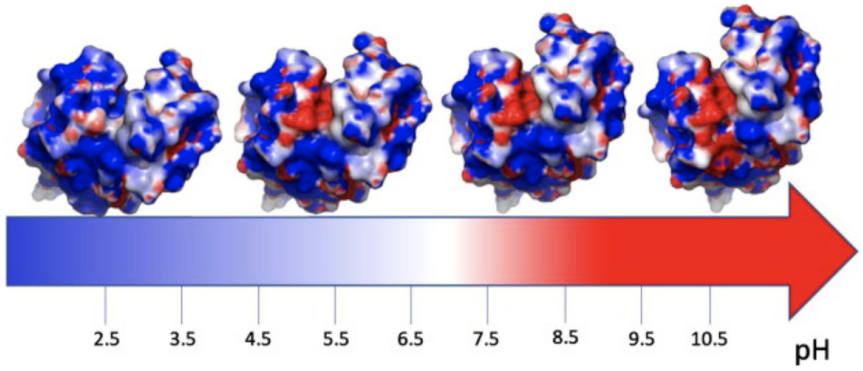

Figure 1.6: Charge distribution of lysozyme at increasing pH (I=0.01 M NaCl). Blue - positive charge, white - neutral, red - negative charge. [5]

In this study, lysozyme and BSA will be used for investigation of protein adsorption mechanisms. Given that characteristics of proteins are important for their adsorption behavior, detailed characteristics of the two will be elaborated.

1.3.2 Lysozyme and BSA

Lysozyme is considered a hard protein which is resistant to structural alterations and denaturation. BSA on the other hand, is a soft protein which undergoes denaturation relatively easily. [47;17] Both proteins are globular, rich in α-helices and contain stabilizing disulfide bonds. [48]

Lysozyome has since its discovering in 1922 emerged as a model protein for studies on protein structure and function, and is today among the most investigated proteins in biochemistry. Hen egg white lysozyme contains a single polypeptide chain with 129 amino acid residues, stabilized by four disulfide bridges. [49] The dimensions of a lysozyme molecule are 3x3x4.5 nm. [10] The protein is easily soluble in aqueous solution, and has an isoelectric point (pI) around 11.1. Characteristics such as easy availability, small size and excellent water solubility make lysozyme a good option. Different regions of lysozyme have shown to dynamically interact with one another. [49]

BSA is another well-characterized and frequently studied protein. It contains 583 amino acid residues and 17 disulfide bridges. BSA consists of three homologous domains, providing various binding sites.[48] The dimensions of a BSA molecule are 4x4x14 nm, and the isoelectric point of BSA is ca. 5.0.[10;46]

1.3.3 Thermodynamics of Protein Adsorption

Generally, a macromolecule in close proximity with a surface will attach to the surface if it is more energetically favorable to interact with the surface than it is to interact with ambient liquid or gas.[50] In other words, proteins will spontaneously adsorb onto a surface if it results in a free energy decrease of the system and surroundings. The change in free energy is expressed in Equation 1.1, where ΔG is change in free energy, ΔH is change in enthalpy, ΔS is change in entropy and T is absolute temperature.[45]

$$\Delta G = \Delta H - T\Delta S \tag{1.1}$$

Protein adsorption at the solid/liquid interface generally occurs due to hydrophobic, electrostatic and/or hydrogen-bonding interactions. Proteins containing both positively and negatively charged amino acids can attach to both positively and negatively charged surfaces.[9]

Protein adsorption can generally be divided into three steps:
1) Transfer of molecules from bulk phase. This step is mainly governed by convection, either due to flow (forced convection) or density differences (natural convection). Alternatively, molecule transfer can be induced by diffusion and external forces.
2) Transfer of particles through the adsorption boundary layer. Diffusion and specific forces between molecules and the interface (and pre-adsorbed molecules) dominate this step.
3) Physical contact formation between molecule and interface (or pre-adsorbed molecules), and immobilization.[51]

For hydrophobic surfaces, the water layer over the surface is in a higher free energy state than water in bulk solution due to unfavorable interactions with the surface. Hence, disreplacement of these water molecules causes a reduction in free energy. Disreplacement of water molecules close to nonpolar areas on the protein surface also contributes to the reduction. Consequently, there is a strong thermodynamic driving force for protein adsorption on hydrophobic surfaces.[45]

On hydrophilic surfaces, proteins must displace hydrogen-bonded water molecules in order to adsorb. There is no change in the overall free energy if a single amino acid displaces water molecules. For proteins with multiple hydrogen-bondable groups, there may be a reduction in the free energy through reduced entropy. Exceptions to this behavior exist, and PEG is an example of such a surface where the bond to the water layer is too strong for proteins to bind.[45]

1.3.4 Protein Adsorption Phenomena

If proteins are structurally stable, their orientation on surfaces may be described as 'side-on' or 'end-on'. The orientations refer to elliptical proteins attached with their long axis or short axis to the surface, respectively. Proteins adsorbed in 'end-on' orientation form a layer with higher thickness than in 'side-on'.[17]

Denaturation of proteins may occur after adsorption to surfaces. Surface coverage of adsorbed proteins is the primary factor for the extent of denaturation. A small amount of proteins of the surface is more likely to spread out until neighboring proteins limit the process. Higher protein concentration in solution allows for less rearrangement of the adsorbed proteins. Surface hydrophobicity also impacts the denaturation process. If interactions between a protein and surface are stronger than the internal structure sustained by hydrogen- and disulfide bonds, the adsorbed protein will be subject to significant structural rearrangement.[47]

Protein adsorption on hydrophobic surfaces is different than adsorption on hydrophilic surfaces. They typically bind stronger to hydrophobic surfaces than hydrophilic, and to charged surfaces than uncharged. Hydrophobic surfaces are thought to destabilize proteins, meaning their secondary structure is more likely to be broken down by hydrophobic interactions. Both lysozyme and BSA have been shown to lose α-helical structures upon adsorption on hydrophobic surfaces.[47;17] Hydrophobic surfaces might also be expected to induce higher-density layers than hydrophilic surfaces, as they are generally regarded as causing protein denaturation. Complete collapse of the protein structure may occur for small proteins.[52]

1.3.5 Interactions in Protein Mixtures

Competitive protein adsorption is one of the more intriguing aspects of protein adsorption on surfaces.[53] It is a general phenomenon that occurs when a protein mixture is adsorbed to a surface. This is commonly referred to as the Vroman effect. The diffusion rates of molecules in protein mixtures vary, and small size and high concentration proteins adsorb first. They may then be displaced by other proteins which are typically of larger size. There are two possible well-accepted partial interpretations of exchange processes in literature. The simplest model describes a situation where an adsorbed protein naturally desorbs from the surface, leaving space for a new protein to adsorb. However, the exchange phenomenon has been observed when introducing multiple proteins to systems where single protein solutions have shown strong enough bindings with the surface to prevent desorption. The time constant for exchange was also found to be inconsistent with the desorption time constant at short timescales, indicating that a faster exchange at shorter time scales must be due to competitive displacement. Proteins capable of displacing already adsorbed proteins have higher surface affinity and are able to adhere more strongly through more surface contacts. This is typically due to characteristics such as large size and conformational flexibility. However, the mechanisms of the process are poorly understood. One possible mechanism involves complex formation, where the new protein embeds itself in the adsorbed protein layer, the complex "turns" and the protein from the adsorbed layer is exposed to the solution and desorbed.[54;55]

Globular proteins may form heteroprotein complexes under favorable conditions. This phenomenon usually occurs when the pH is between the pI values of positively and negatively charged proteins. The complexes are highly sensitive to pH and ionic strength variations, indicating that electrostatic interactions is the dominant driving force. However, hydrophobic and dipolar interactions may also contribute. The BSA protein used in this study contains different domains which may function as active binding sites for smaller molecules such as lysozyme.[46]

1.3.6 Quantification of Protein Adsorption

There are various approaches for quantification of protein adsorption, of which one of the most popular is constructing an adsorption isotherm. The method is simple, and includes plotting amount of adsorbed protein as a function of solution concentration. The shape of the isotherm can then provide information about the thermodynamics of the adsorption. The Langmuir, Freundlich and Brunauer-Emmett-Teller (BET) isotherm models are examples of models used to describe protein adsorption. Different principles and requirements are used for the different models. The characteristic shape of the respective models are presented in Figure 1.7.[6]

The Laungmuir and Freundlich models are based on assumptions of monolayer formation. Langmuir assumes that all adsorption sites have the same adsorption energy, while Freundlich assumes different adsorption energies and rates for different adsorption sites. Multilayered adsorption is provided for by the BET model.[6]

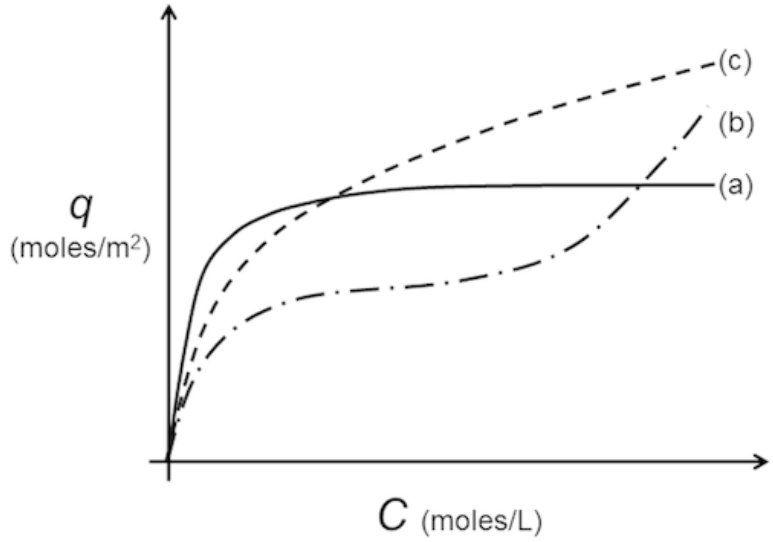

Figure 1.7: Characteristic shapes of adsorption isotherm models (a) Langmuir isotherm, (b) BET isotherm and (c) Freundlich isotherm.[6]

1.3.7 Self-assembled Monolayers (SAMs)

Self-assembled monolayers (SAMs) are increasingly used in applications related to biofouling research, and SAMs of organic thiolates have proven to be useful for studies of protein adsorption and other surface interaction phenomena.[7;56] Adsorption of alkanethils on gold and other metal substrates is the most extensively studied class of SAMs.[7;57;58]Excellent model systems for protein interactions with organic surfaces can be obtained through forming SAMs of long-chain alkanethiolates on gold films. The interfacial properties of the monolayers such as hydrophobicity/hydrophilicity can be controlled by changing the tail group.[59;60]

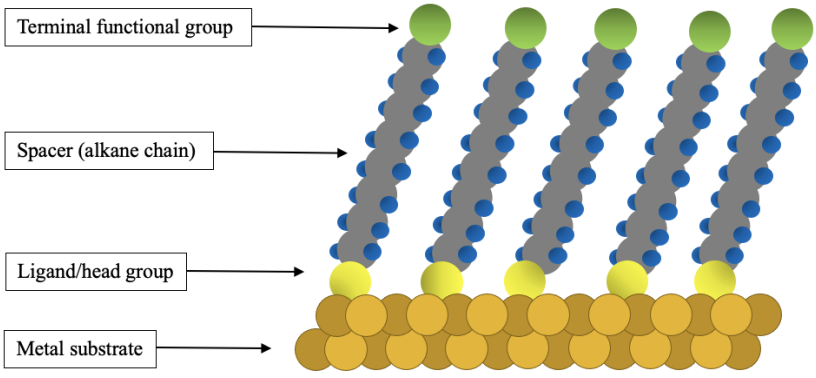

Figure 1.8: Sketch of SAM of an alkanethiolate adsorbed on a gold surface. Modified from[7].

The most common protocol for SAM deposition on gold and other metals is immersion of a freshly prepared or clean substrate into an ethanolic solution of thiols (∼1-10 mM) for 12-18 h. The adsorbates densely cover the substrate within milliseconds to minutes, but this is followed by a slow reorganization process. Hence, it takes hours to obtain maximize the density and minimize defects. Factors such as temperature, solvent, concentration, immersion time, purity of adsorbate and cleanliness of substrate can affect the formation rate and the structure of the SAM.[7]

The roughness and cleanliness of the substrate are crucial parameters for the quality of the monolayer.[61] There has not yet been developed a general method for convenient monolayer removal, but etching with piranha solution and plasma cleaning are two common methods. Oxygen is a chemically reactive gas which reacts with the monolayer and forms gaseous product during the plasma cleaning.[62] Organic contaminants on the surface are converted to CO, CO_2, CH_4 and H_2O.[63] These fragments should be swept away by the continuous gas flow so that no further cleaning is necessary.[62] Oxygen plasma treatment is reported to oxidise the gold surface, which may affect the properties of the monolayer. Reduction of gold oxide formed during plasma cleaning can be obtained through reaction with ethanol.[61;63] Piranha cleaning and plasma cleaning ideally achieve the same level of cleanliness, but results obtained by Cha et al.[63] suggest that slightly cleaner surfaces are obtained from plasma cleaning.

1.3.8 Surface Wetting and Contact Angle Measurements

Analysing the contact angle a liquid forms on a surface can determine wetting properties of the surface, i.e. if a surface is hydrophobic or hydrophilic. When using water as the wetting liquid, hydrophilic surfaces yield a contact angle of $<90°$, while the contact angle of hydrophobic surfaces are $>90°$.[64] Droplet volume has no significance on close-to-ideal substrates.[65]

The wettability of a surface depends on areal interfacial free energy at the solid-vapor (γ_{sv}), solid-liquid (γ_{sl}) and liquid-vapor (γ_{sv}) interfaces, as displayed in Figure 1.9. The behavior of a liquid phase in contact with a solid surface can be described using Young's equation (Equation 1.2):[66;67]

$$Cos\theta = \frac{\gamma_{sv} - \gamma_{sl}}{\gamma_{lv}} \tag{1.2}$$

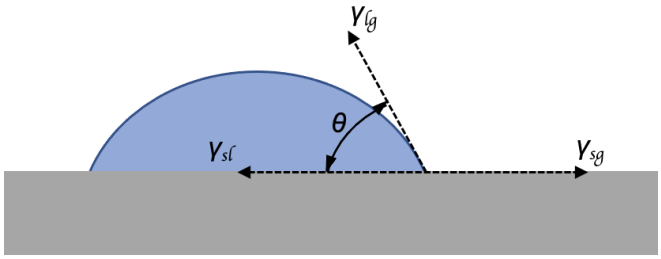

Figure 1.9: Contact angle...

Despite extensive use of gold in research, wettability and other surface properties continue to raise ambiguity in literature.[68]

Canning et al.[68] state that contact angles are typically reported to ∼66° or ∼76° on gold films, but that variations are also reported. Various cleaning procedures including UV/Ozone cleaning and oxygen plasma cleaning generate highly hydrophilic surfaces, which suggests presence of gold oxide. They argue that these superhydrophilic contact angles on gold are caused by gold oxidation or unclean environments.

Smith[69] presented an overview of water contact angle on gold obtained in previous experiments. 18 references concluded with a contact angle over 30 °, while 8 references report a contact angle close to 0°. In cases where conclusion was $\theta>30$, authors suggest the opposite conclusion is attributed to hydrophobic contamination by organic contaminants. Researchers concluding with θ ∼0, on the other hand, argue that the opposite conclusion results from hydrophilic contamination of oxygen or oxides on the surface. The authors of the comparative article concluded, based on Auger electron spectroscopy, that clean gold has a contact angle ∼0.

Paulik et al. [70] obtained contact angles between 76° and 83° on bare gold. Zina et al. [71] measured a contact angle of 81° on gold, which was reduced to 49° after piranha cleaning of the surface. [71]

Contact angles on different polymer SAMs also varies in literature. Gupta et al. [56] obtained contact angles of 71° on gold, 33° on 11-hydroxyundecane-1-thiol (-OH) and 112° on dodecanethiol (-CH_3). Yuan et al. [72] obtained contact angle 106° on 1-undecanethiol (-CH_3) and 22° on 11-mercapto-1-undecanol(-OH). Contact angle was measured to 114° of hexadecanethiol (-CH_3) on gold sensors by Hedin et al. [73].

Phan et al. [9] measured contact angles of 23° on 11-mercapto-1-undecanol (-OH), 25° on 11-mercaptoundecanoic acid (-COOH), 97° on 1-decanethiol (-CH_3) and 48° on 11-amino-1-undecanethiol hydrochloride (-NH_2). Jernstrom [61], on the other hand, obtained contact angles of 15° for 11-mercaptoundecanoic acid (-COOH) and 10° for 11-mercapto-undecanol (-OH). Like Phan et al. [9], they also measured an angle of 97° on 1-undecanethiol (-CH_3).

1.3.9 Adsorption Studies using QCM-D

Characteristics such as high sensitivity, fast response, real-time detection, easy operation and low experimental cost has made quartz crystal microbalance (QCM) a widely used tool for various biological analyses. [74] QCM essentially is a nanoscale balance capturing changes in mass on a surface as molecules adsorb or desorb. Voltage is applied to a crystal so that it is excited to resonance, and changes in the resonance frequency are detected. These changes can be converted to mass and thickness of the adsorbed layer. The mass detected by QCM includes mass of solvent associated with adsorbed molecules, and is often referred to as hydrated mass. [8]

The relation between frequency and mass was identified in 1959 by Gunther Sauerbrey, yielding the Sauerbrey equation (Equation 1.3). It states a linear relation between the resonance frequency of on oscillating quartz crystal and changes in mass. C is the mass sensitivity constant, related to the properties of quartz. For a 5 MHz quartz crystal, C is 17.7 ng/(cm^2· Hz). n is the number of the harmonic used (1, 3, 5, 7, ...). The linear relation is based on the characteristics of a pure quartz crystal, meaning the adsorbed layer has to be similar so that it can be approximated to be part of the crystal. Hence, the relation is only valid for thin, rigid and firmly attached layers. [75] Use of the Sauerbrey equation for soft or viscoelastic films on the sensor surface can lead to and underestimate of the mass adsorbed. [50]

$$\Delta m = -C \cdot \frac{\Delta f}{n} \tag{1.3}$$

QCM-D is an extension of QCM that also detects changes in energy loss, which gives insight into the system's viscoelastic properties. Structural changes of the adsorbed layer such as crosslinking, swelling and collapse can be detected. [8] A rigid layer results in increased decay time, and therefore low dissipation. On the other hand, a viscoelastic layer will give fast damping of the crystal and consequently short decay time and high dissipation. [76] For viscoelastic layers, viscoelastic models such as the Voigt model can be used. This model assumes a uniform viscoelastic film in contact with a Newtonian liquid under no-slip condition. [73]

In the case of mass adsorption on the sensor surface, the frequency decreases and dissipation increases. Figure 1.10 displays a typical frequency and dissipation diagram obtained from QCM-D measurements.

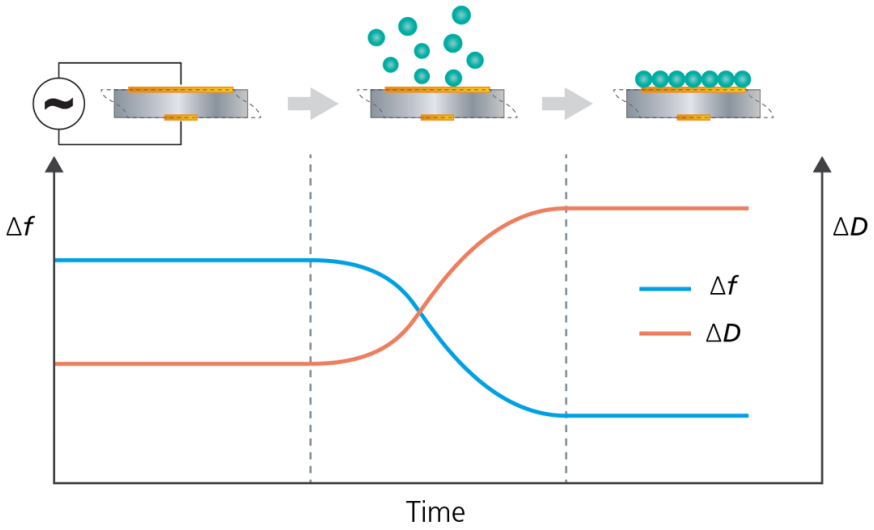

Figure 1.10: Schematic of adsorption and resulting QCM-D diagram with a decrease in frequency and increase in dissipation. [8]

1.3.10 Previous Studies on Protein Adsorption Using QCM-D

Protein adsorption on SAMs was also studied by Sigal et al. [10]. There was a general trend of increased adsorption with decreased wettability. They discovered that smaller proteins were much less sensitive to the wettability of the surface than larger proteins. There was significant adsorbance of smaller proteins even on the most wettable surfaces.

Jernstrom [61] formed SAMs of MUA, MUOH and DT10 and studied protein adsorption on the formed monolayers using surface plasmon resonance (SPR). Interestingly, their findings revealed a higher degree of adsorption for BSA compared to lysozyme across all surfaces examined. These results suggest that smaller proteins exhibit greater sensitivity to surface wettability than larger proteins, which contradicts the observations reported by Sigal et al. [10].

Phan et al. [9] studied adsorption of bovine serum albumin (BSA) onto SAMs using QCM-D and spectroscopic ellipsometry (SE). The SAM surfaces studied were 11-mercapto-1-undecanol (MUOH), 11-mercaptoundecanoic acid (AUT), 1-decanethiol (DT10) and 11-amino-1-undecanethiol hydrochloride (AUT). They observed a thicker layer and more densely packed BSA molecules on charged surfaces than neutral surfaces. Adsorption on both charged surfaces was similar in terms of film thickness, amount of molecules adsorbed and porosity. The initial adsorption rate was higher on the positive surface than the negative. It was argued that adsorption onto the similarly charged surface (MUA) was attributed to electrostatic interactions between positively charged residues in the protein molecule and the negatively charged surface.

Yu et al. [18] studied lysozyme adsorption on six different surfaces using simulations. Surfaces were hydrophobic (CH_3-SAM-like), neutral hydrophilic (OH-SAM-like and OEG-like SAM), zwitterionic (SB-like SAM), negatively charged (COOH-SAM-like) and positively charged (NH_2-SAM-like). Results indicate less structural changes on hydrophilic (OH-SAM) than hydrophobic (CH_3-SAM), likely because hydrophobic residues inside the protein are exposed to the hydrophobic surface. Lysozyme adsorbed in a 'end-on' configuration on the hydrophobic surface and 'side-on' on hydrophilic. The switterionic surface resisted lysozyme adsorption, and no stable adsorption occurred on the OEG-surface. OEG showed stronger protein resistance properties than the other neutral hydrophilic polymer (-OH), attributed to stronger hydrophilic property and further, a stronger hydration layer over the surface. Effect of ionic strength on adsorption onto charged surfaces was also investigated with NaCl. Results show that an ion layer is formed near the surface at high ionic strength. This allowed for lysozyme adsorption on both positively and negatively charged surfaces, while lysozyme only adsorbed on the

negatively charged surface at low ionic strength conditions. They argue that lysozyme did not adsorb on the positively charged due to electrostatic repulsion between similarly charged protein and surface.

Hedin et al. [73] studied adsorption of the polymer ethyl(hydroxyethyl)cellulose on hydrophobic surfaces. Due to reproducibility issues with the absolute values of the adsorption, QCM-D measurements were repeated until at least 2 out of 5 results (F and D) differed less than 10%. Trends were, however, the same in all experiments. This highlights reproducibility issues related to this type of experiments. Standard deviations were also large for Phan et al. [9] who performed three repetitions of BSA adsorption on SAMs.

2 Materials and Methods

In this section, firstly the chemicals used during experimental work are listed. Further, experimental procedures are explained. The experimental work is separated into three parts:

1) Sensor cleaning and characterization
2) SAM formation and characterization
3) Protein adsorption studies on SAMs using QCM-D

2.1 Materials

Chemicals used during the work of this project are presented in Table 2.1. All chemicals were used as received without further purification. MQ-water used in experiments was produced by Simplicity Millipore water purification system. Artificial seawater contains all salts found in natural seawater at concentrations >0.0004%, detailed composition is specified in Appendix A.1.

Table 2.1: Chemicals used in experiments procedures with CAS number.

Chemical	CAS Number
11-Mercapto-1-undecanol (97%)	73768-94-2
11-Mercaptoundecanoic acid (95%)	71310-21-9
11-Amino-1-undecanethiol, hydrochloride (<100%)	143339-58-6
1-Decanethiol (99%)	143-10-2
Bovine serum albumin (≥98%)	9048-46-8
Lysozyme (≥95%)	12650-88-3
Sodium dodecyl sulfate (≥97%)	151-21-3
Ethanol absolute (≤100%)	64-17-5
Sulfuric acid (95-97%)	7664-93-9
Hydrogen peroxide (30%)	7722-84-1
Ammonia (25%)	1336-21-6
Artificial seawater	
Nitrogen (5.0)	

2.2 Sensor Cleaning

Two different methods were used for sensor cleaning. After each cleaning procedure, contact angle was measured to characterize the cleanliness of the surface. Details on contact angle measurements are presented in Section 2.4 It was initially performed according to method 1, where 3 variations of the method were tested. Based on results obtained by contact angle measurements after cleaning, a new method was adapted. Sensor cleaning was initially done according to method 1. Contact angle measurements after this procedure indicated that sensors were not clean after this treatment. Method 2 was therefore used prior to SAM formation for all experiments.

Initially, sensors were cleaned according protocol A-I by Biolin Scientific,[77] with some modifications. Figure 2.1 displays a schematic of cleaning method 1. Detailed steps are described below. The cleaning procedure was performed in two labs, where nitrogen drying and UV/Ozone cleaning was performed at a different laboratory from chemical solution cleaning.

Method 1
1) UV/Ozone treat sensor for 10 minutes.
2) Heat a 5:1:1 mixture of MQ water, ammonia (25%) and hydrogen peroxide (30%) to approx. 75 ℃.
3) Immerse the sensor in the heated solution for ca. 30 minutes.

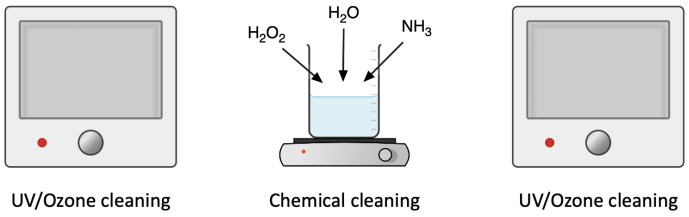

Figure 2.1: Schematic showing cleaning method 1.

4) Rinse with copious amounts of MQ water.
5) Dry sensor with nitrogen gas.
6) UV/Ozone treat sensor for 10 minutes.

Sensor cleaning was performed in a different laboratory than nitrogen drying, and 3 variations of method 1 were tested to investigate if the wettability of the gold surface was affected by how the sensor was handled between step 3 and 5. Variations were:
i) No rinsing with MQ water after chemical cleaning (skip step 4).
ii) Sensors rinsed with MQ water and stored in air for 5-10 min before drying with nitrogen.
iii) Sensors rinsed with, and stored in, MQ water for 5-10 min before drying with nitrogen.

After varying and unreliable results from method 1, method 2 was adapted. This includes procedures commonly used for monolayer removal on gold surfaces.[62] The entire procedure was performed at the cleanroom facilities of NTNU NanoLab. A schematic of cleaning method 2 is displayed in Figure 2.2.

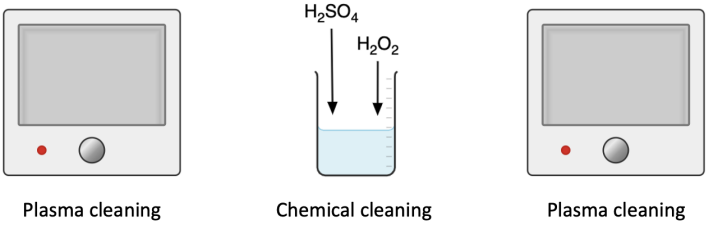

Figure 2.2: Schematic showing cleaning method 2.

Method 2
1) Oxygen plasma clean sensor for 5 minutes.
2) Mix a 3:1 solution of sulfuric acid (95-97%) and hydrogen peroxide (30%) by adding hydrogen peroxide slowly to sulfuric acid.
3) Immerse sensor in solution for ca. 30 minutes.
3) Rinse with copious amounts of MQ water.
4) Dry sensor with nitrogen gas.
5) Oxygen plasma clean sensor for 5 minutes.
6) Immerse sensor in ethanol.

Sensors were cleaned according to method 2 immediately prior to SAM formation.

2.3 Preparation of Self-assembled Monolayers

SAMs were formed of 4 different alkanethiols representing different types of environmentally relevant surfaces with different charge and wettability. One polymer was hydrophobic, while the 3 other were hydrophilic with different charges. This enabled both effect of wettability and charge to be investigated. Characteristics of the polymers are presented in Table 2.2.[9]

Table 2.2: Characteristics of investigated SAMs. Modified from Phan et al. [9].

Abbreviation	Chemical name	End group	Features	Charge at pH 7
MUOH	11-Mercapto-1-undecanol	-OH	Hydrophilic	Neutral
MUA	11-Mercaptoundecanoic acid	-COOH	Hydrophilic	Negative
AUT	11-amino-1-undecanethiol, hydrochloride	$-NH_2$	Hydrophilic	Positive
DT10	1-Decanethiol	$-CH_3$	Hydrophobic	Neutral

Four sensors were immersed into 2 mM solutions of the each alkanethiol in absolute ethanol for at least 18 hours. Ultrasonication was used to dissolve MUOH. A fresh bottle of absolute ethanol was used in all experiments.

Prior to characterization, the sensors were thoroughly rinsed with ethanol and dried with nitrogen. Sensors were stored in the alkanethiol solutions between characterization and QCM-D experiments.

2.4 Characterization Using Contact Angle Measurements

Contact angle measurements were used for characterization of surfaces both after chemical cleaning (gold surface) and after SAM formation (polymer surface).

Contact angle was measured using Kruss DSA25 and Advance software. Sessile drop method was used. 5 µL droplets were placed on the surface by a micro-syringe. The static contact angle (θ_s) was determined in all cases, and 5 or more measurements were performed on each sensor. Automatic baseline was used on hydrophilic surfaces (gold and hydrophilic polymers), while a manual baseline was used on hydrophobic surfaces since the software struggled to place the baseline correctly.

2.5 Protein Adsorption Studies Using Quartz Crystal Microbalance with Dissipation (QCM-D)

Protein adsorption was monitored in real-time using *in-situ* QCM-D. Lysozyme and bovine serum albumin (BSA), two proteins with different charge and size, were used to study protein adsorption on the surfaces. Characteristics of lysozyme and BSA are presented in Table 2.3.

Table 2.3: Characteristics of proteins used in adsorption studies. Modified from [10].

Protein	MW (kD)	pI	Net charge at pH7
Lysozyme	14	11.1	+
BSA	69	4.8	-

The protein solutions used in the QCM-D experiments are presented in Figure 2.3. For all experiments, proteins were dissolved in artificial seawater(ASW) to mimic marine environment. A sequential deposition with increasing lysozyme concentration was performed for concentrations in the range 10-3000 ppm. Adsorption of single protein solutions of lysozyme and BSA were studied, in addition to a binary mixture of lysozyme and BSA.

The protein solutions were adsorbed onto the gold sensors coated with different SAMs discussed in Section 2.3. Figure 2.4 shows a schematic displaying the properties of the investigated SAMs.

The four different protein solution variations were all adsorbed onto the four different sensors, resulting in a total of 16 QCM-D experiments.

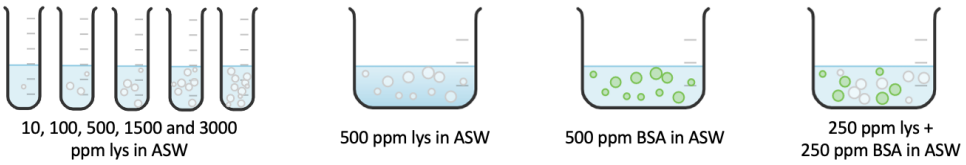

Figure 2.3: Protein solutions used in QCM-D experiments.

Figure 2.4: Surface properties of SAMs used in QCM-D experiments. Blue color represents hydrophilic surfaces, and red hydrophobic. +, - and 0 represent positively, negatively and neutrally charged surfaces, respectively.

Flow rate was set to 50 µL/min. Harmonics were evaluated in air and MQ water prior to every experiment. MQ water was run for 5 minutes at the beginning of each experiment, before running artificial seawater (ASW) until a stable baseline was reached. The respective protein solution was then introduced into the flow cell until equilibrium was reached. For the longest experiments, the protein solutions were run until the frequency decreased with less than 5 Hz in 10 min. ASW was then pumped into the cell to remove any passively attached protein molecules.

The setup for QCM-D experiments is shown in Figure 2.5. Solutions were pumped through a chamber where the sensor was placed using a peristaltic pump, before ending up in a waste cup.

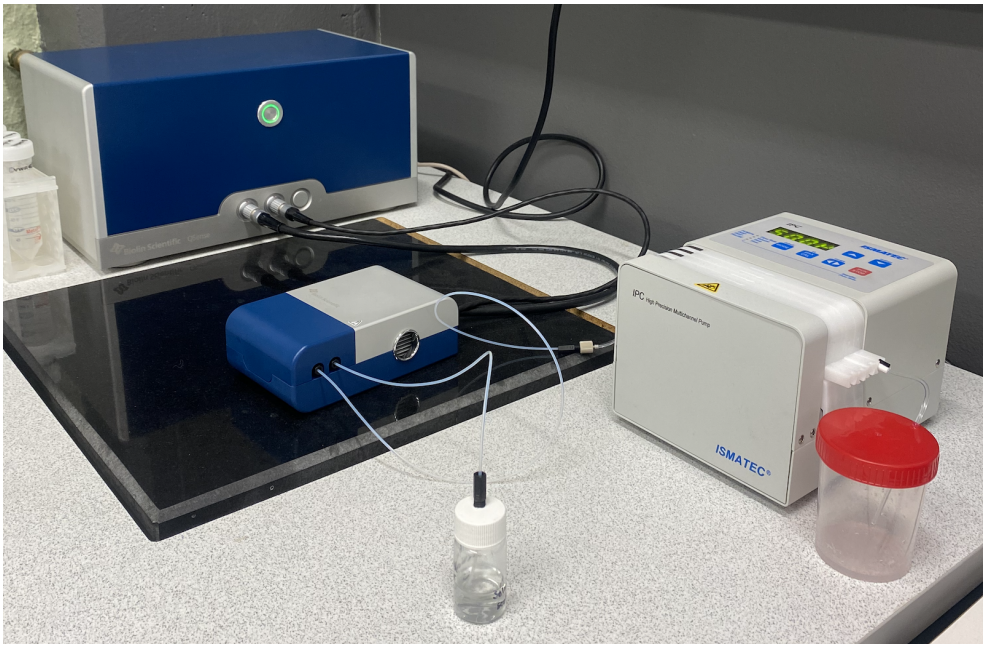

Figure 2.5: Setup for protein adsorption using QCM-D.

After experiments, the liquid path was cleaned according to protocol "After experiments with proteins and peptides" by Biolin Scientific, with modifications: [77]

1) Prime the fluid path with MQ water.
2) Flush the fluid path with 2% SDS.
3) Pause the priming sequence for 30 minutes.
4) Flush the fluid path with MQ water. for ca. 10 minutes.
5) Flush the fluid path with air for ca. 5 minutes.
6) Dry the fluid path using nitrogen gas.

The software QSense Dfind by Biolin Scientific was used to process data from experiments. Sauerbrey could not be used as the formed layers were too viscoelastic. Two modeling principles "Dfind Smartfit" and "Dfind Broadfit" were used.

Smartfit is well suited for measurements with significant D shifts and/or well separated frequency shifts for the different harmonics. The model typically finds a solution for a rigid thin layer and a soft thick layer, whereof one of the solutions usually has a better fit quality than the other. It tries to track solutions, and is constrained within solution sets. If this method fails to provide good fit solutions, Broadfit may be a good option. This model is not constrained within solution sets, and searches for the best fit of the measured data in each individual point. [78]

The fit quality of the models provides an idea of how well the modeled results fit the measured values. It is based on the average of the normalized deviation between calculated and measured f and D values. It is a value between 0 and 1, where 0 means poor overlap and 1 means excellent overlap between calculated and measured values. [78]

The adsorbed layer was assumed to be a hydrated protein layer with density 1100g/L.

3 Results and Discussion

In this section, results from the conducted experiments will be discussed. The first section focuses on the development of a reproducible cleaning procedure for the gold sensors. Moving forward, the second section focuses on the evaluation of self-assembled monolayers (SAMs) on the gold sensors. Following, there is extensive discussion of the protein adsorption experiments conducted on the SAM-coated sensors. Comprehensive analysis and evaluation of mass, thickness and viscoelastic properties were carried out for all experimental conditions. In attempts to gain insights into the dynamic protein-surface interactions, the kinetic factor adsorption rate was also evaluated. At last, effect of protein concentration was examined through constructed adsorption isotherms.

3.1 Cleanliness of the Sensor Surface

The establishment of an effective and reliable cleaning protocol was a significant focus of this master's thesis. Recognizing the critical importance of substrate cleanliness and roughness in achieving high-quality monolayers, considerable effort was dedicated to developing a robust and reproducible cleaning procedure. A systematic investigation of various cleaning techniques, including chemical solutions, UV/Ozone and plasma treatments, was conducted to ensure optimal sensor condition for subsequent experiments.

In this study, four sensors were employed, all of which had been previously used in other experiments prior to the commencement of this project. Consequently, there might have been minor defects in the gold layer. To evaluate the cleanliness of the gold sensors, contact angle measurements were employed as a characterization technique.

An angle of $<5°$ is usually hard to detect by software during contact angle measurements. In this project, a higher threshold was set for contact angle measurements. When dealing with angles lower than approximately 10 degrees, the software often faced difficulties in accurately detecting the droplet on the surface. In cases where a baseline was detected for these low angles, the measured values exhibited significant variability within seconds without any apparent trend. For measurements where the angles were too low for the instrument to provide accurate results, results will be presented as too low to measure (TLTM). Based on literature, it was determined that a contact value of TLTM would indicate a clean surface and larger angles indicated contamination.

Furthermore, an additional challenge encountered at low angles was the asymmetry of the droplets, as evident in Figure 3.1. Any variation in the rotation of the sensors relative to the camera would naturally lead to variations in the measured angles. It is worth considering that the use of 5 µL droplets might have contributed to these issues, and employing smaller volumes could potentially yield more reliable results.

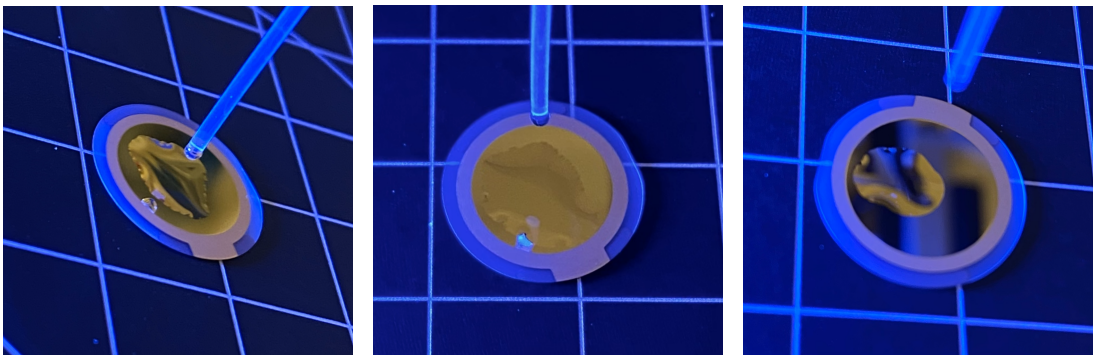

Figure 3.1: Unsymmetrical droplets on sensor surface during contact angle measurements.

Initially, UV/Ozone cleaning, chemical cleaning and contact angle measurements were performed at different departments located in different buildings. The chemical cleaning and water rinsing procedures were conducted in a different laboratory than the nitrogen drying step. Consequently, the sensors were stored in a closed container for a period of 5-10 minutes prior to nitrogen drying. There was speculation that this particular sequence of steps could have potentially influenced the outcomes of the experiment. Therefore, in order to address this concern, three different variations of the post-chemical cleaning procedure were investigated as described in Section 2.2.

Results from the three variations in method 1 are presented in Table 3.1. Two sensors were cleaned each time, and at least 10 measurements were done on each of them.

Table 3.1: Contact angle (°) of variations 1, 2 and 3 of cleaning method 1.

Variation	Sensor 1	Sensor 2
1	4 x TLTM - 20°	∼12°
2	TLTM	TLTM - 23°
3	∼11-17°	∼10-19°

Contact angles were relatively low on all surfaces, indicating relatively clean surfaces for all variations. For the procedure without water rinsing (1), contact angles on sensor 1 were initially TLTM, but increased to ∼20° during the procedure. On the second sensor, the angle was stable at around 12°. After sensors were stored in air before nitrogen drying (2), one of the sensors exhibited contact angles TLTM, while contact angle on the second sensor increased from TLTM in the first measurement to 23° in the last. For the sensors stored in MQ water (3) between chemical cleaning and UV/Ozone treatment, angles varied between 11-17° on sensor 1, and 10-19° on sensor 2. Based on these findings, it was determined that the second variation (2), involving rinsing the sensor with water and subsequently storing it in air before drying, would be the preferred approach moving forward. Both of these sensors initially exhibited values TLTM.

Two sensors were then cleaned according to this variation three times. 10 parallels of contact angle measurements were performed on each of the two sensors. Results are presented in Table 3.2.

Table 3.2: Contact angle (°) of variations 1, 2 and 3 of cleaning method 1.

	Sensor 1	Sensor 2
1	3 x TLTM, ∼18-71°	3 x TLTM, ∼10-25°
2	∼24°	∼25°
3	TLTM	TLTM

The first time, the angle was TLTM in the 3 first parallels. For sensor 1, the angle then exhibited values between 18° and 71° without an apparent trend, while sensor 2 varied between 10° and 25° . This indicated that the surfaces were contaminated during the contact angle measurements.

The second time, contact angles were stable throughout the measurements. They were measured to 24.1 ± 3.5° and 25.4 ± 3.2° on the two sensors, indicating that the surfaces were not adequately cleaned.

During the third round of measurements, angles were too low to measure on both sensors in all of the measurements. It was finally concluded that the surface was sufficiently clean. However, due to the inconsistent contact angles obtained in each of the three experiments, it was determined that the method lacked reproducibility and could not be utilized reliably.

Considering the inconsistent angles throughout the experimental trials, the decision was made to conduct the entire procedure within the controlled environment of Nanolab's cleanroom facilities, aiming to reduce the risk of potential contamination. Furthermore, it was hypothesized that the treatment employed might be insufficient to eliminate polymers and proteins irreversibly adsorbed onto the sensors. Consequently, from this point forward, method 2 was adopted. The effect of plasma and piranha cleaning was also studied using contact angle measurements.

Contact angle measurements were performed after each step in method 2. After the first plasma cleaning, contact angles were TLTM. After the piranha cleaning procedure, the contact angle measured approximately 60 degrees before reverting back to TLTM after the second plasma cleaning. Contact angle of a clean gold surface varies greatly in literature, but it was decided that TLTM was considered clean. Since formation of a gold oxide layer by plasma cleaning is reported, the sensors were immersed in absolute ethanol after this process.

Results obtained using method 2 were satisfying and reproducible, and this method (plasma-piranha-plasma) was performed prior to SAM formation.

3.2 Formation of Self-assembled Monolayers (SAMs)

After cleaning sensors according to the method described above, they were immersed in ethanolic alkanethiol solutions to form SAMs.

Two repetitions of SAM formation and contact angle measurements on the 4 sensors were performed prior to QCM experiments to get an indication of the reproducibility. Average contact angles and standard deviations from 20 measurements (5 measurements x 4 sensors) are presented in Figure 3.2. Contact angles on each of the sensors in both experiments are attached in Appendix A.2.

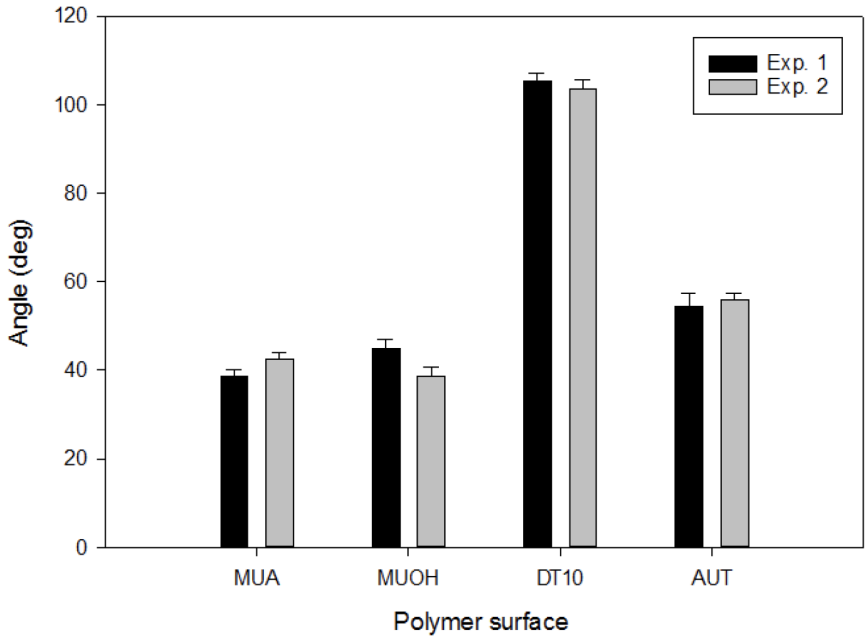

Figure 3.2: Contact angles on SAM surfaces of MUA, MUOH, DT10 and AUT. Presented values for each measurement are averages of 4 sensors with 5 measurements each.

In general, the reproducibility was given on all SAMs. However, that is only based on duplicate measurements. The biggest deviation between repetition 1 and 2 was observed on MUOH, where the average contact angle was 6.2 degrees higher the first time compared to the second.

Formation of SAMs on gold has been investigated in multiple studies with inconsistent results. In this experiment, contact angles on all SAM surfaces were higher than results obtained by Phan et al. [9]. However, trends are the same. The contact angles of MUA, MUOH and AUT were less than 90°, indicating hydrophilic-terminal SAMs. MUA and MUOH exhibit similar angles, while the angle of AUT is slightly higher. DT10 is the only SAM exhibiting a contact angle >90°, indicating a hydrophobic-terminated SAM.

Various factors including temperature, solvent, concentration, immersion time, purity of adsorbate and cleanliness of substrate affect the resulting SAMs. [7] To ensure optimal conditions, a newly opened bottle of absolute ethanol was consistently utilized in all experiments. Considering the implementation of a standardized cleaning procedure prior to SAM formation, it was assumed that the substrates were sufficiently clean before being immersed in polymer solutions.

Wettability measurements are affected by both surface topography and surface chemistry. Root mean square (rms) roughness of the gold sensors is 0.9 ± 0.2 nm. [79] Considering the variations in surface roughness are small, it is assumed that surface chemistry is the dominant factor in determining contact angles. Despite the small surface roughness variations, bigger variations may have occurred through defects as a result of previous experiments.

For hydrophilic surfaces, an automatic baseline was applied consistently throughout the measurements. It was monitored that the detected baseline was correct. In the case of the hydrophobic polymer, however, the software encountered difficulties in accurately determining the appropriate baseline. It was therefore placed manually. The solid-liquid interface was easily observed on all investigated surfaces, and both automatic and manual baselines should provide accurate results.

Contact angle measurements indicate successful polymer adsorption on the gold surfaces. However, these measurements do not exclude the possibility of a discontinuous/partial monolayer. To gain further insights into the polymer layer, complementary techniques such as spectroscopic ellipsometry (SE) and x-ray photoelectron spectroscopy (XPS) could be employed.

3.3 Protein Adsorption on SAMs Using QCM-D

In this section, different properties of the adsorbed layer are presented and discussed. Results are typically presented for lysozyme first, followed by BSA and lysozyme/BSA. For all experiments the sequence was MQ water - ASW - protein solution - ASW. These distinct stages are visually represented by grey lines in relevant diagrams.

The effects of surface roughness and thickness on protein resistance have not been taken into consideration in this analysis. It is worth mentioning that the alkanethiols studied share a similar carbon chain length, enabling the attribution of differences in adsorption behavior to the distinct terminal functional groups.

It is important to emphasize that the QCM-D experiments in this study were conducted as single measurements due to time limitations, and as a result, the reproducibility of the results remains unknown. Another consequence of time limitations is that sequential depositions were only performed for lysozyme.

3.3.1 Changes in Frequency and Dissipation During Adsorption

Upon data processing in the software, the frequency and dissipation of artificial seawater were set as reference. In this way, the results obtained from the software stem only from protein adsorption, and the increase in mass and other parameters as a result of salt addition to the system are not considered. Since frequency decreased when switching from MQ water to ASW, the frequency is positive at the beginning of the diagrams as it is positive relative to the one of ASW. Dissipation, on the other hand, increased when ASW was introduced, yielding negative

initial values for dissipation. The 3rd, 5th and 7th overtones are presented in the diagrams, and were used to estimate parameters such as mass and thickness.

Lysozyme Adsorption

As displayed in Figure 3.3, frequency and dissipation diagrams from lysozyme adsorption experiments were similar on all surfaces. Frequency shifts observed for the 3rd, 5th, and 7th overtone ranged between -110 and -140 in all experimental trials. Additionally, the dissipation shifts recorded were consistently within the range of 14-20 ppm.

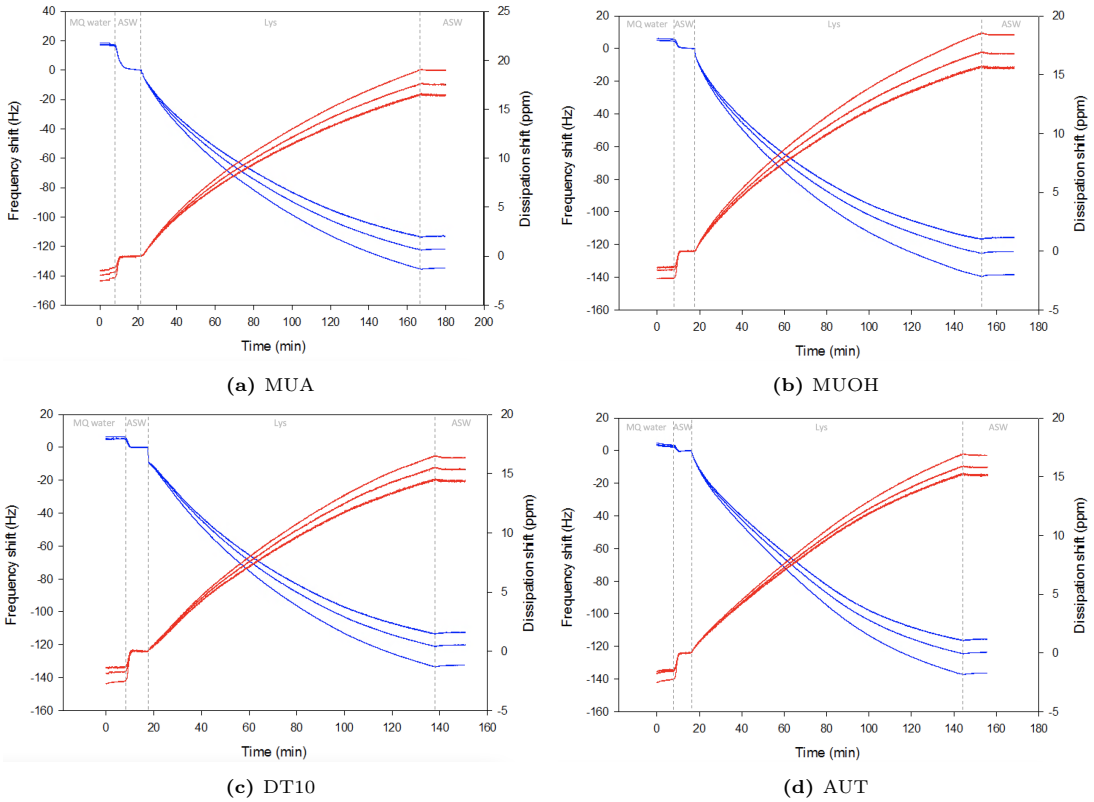

(a) MUA **(b)** MUOH

(c) DT10 **(d)** AUT

Figure 3.3: Frequency and dissipation diagrams of lysozyme adsorption on polymers. Blue and red graphs represent frequency and dissipation (overtones 3, 5 and 7), respectively.

Upon rinsing with ASW, minor variations in frequency and dissipation were observed. This will be examined and discussed further in relation to factors such as mass, thickness and viscoelastic behavior. The similar frequency and dissipation-diagrams suggest that the adsorption process may depend on other factors than the surface properties under the set conditions.

Phan et al.[9] obtained significantly more protein adsorption on the charged surfaces than both uncharged surfaces. However, they dissolved the protein in DI water, meaning no or very few ions were present in solution. In the ASW solution, both mono- and divalent ions were present. The presence of ions in the ASW solution likely led to the formation of an electric double layer on the hydrophilic surfaces, thereby reducing the impact of surface properties on protein adsorption. Upon the introduction of the ASW solution to the system, a decrease in frequency and an increase in dissipation were observed. This suggests that the ions present in the dissolved salts adsorbed onto the surface, resulting in changes in the viscoelastic behavior of the system.

The adsorption of lysozyme on these surfaces was found to be a relatively slow process. Upon introducing the solution, there was either no initial steep slope or only a very short section exhibiting such behavior. Instead, the frequency graphs displayed a gradual and slow decrease

in slope throughout the majority of the adsorption process. Due to the prolonged duration of the adsorption process, experiments were terminated at a pre-defined slope value as a practical consideration.

BSA Adsorption

In the case of BSA, more pronounced variations were observed in the frequency and dissipation diagrams for the different surfaces, as depicted in Figure 3.4. This is in agreement with observations by Sigal et al. [10], where bigger proteins were more sensitive to variations in surface wettability.

The adsorption of BSA onto the surfaces was found to occur rapidly, with the majority of the frequency decrease taking place within the first few minutes. This indicates that BSA has high affinity toward the surface. Another possibility is that BSA was unstable in the solution. However, it should be stable under the experimental conditions chosen.

Compared to lysozyme, the changes in frequency and dissipation were significantly smaller for BSA adsorption, suggesting a lower mass adsorption on the surface. Since the adsorption process is fast, and the small changes in frequency upon rinsing with ASW suggest strong, irreversible bonds to the surface, it may not be argued that surface affinity is low. It is hypothesized that BSA adsorption stopped at monolayer formation, and that lysozyme continued to form multilayers. This will be further discussed in the next sections.

Notably, the frequency exhibited the most pronounced decrease on the oppositely charged AUT surface, likely attributed to electrostatic interactions.

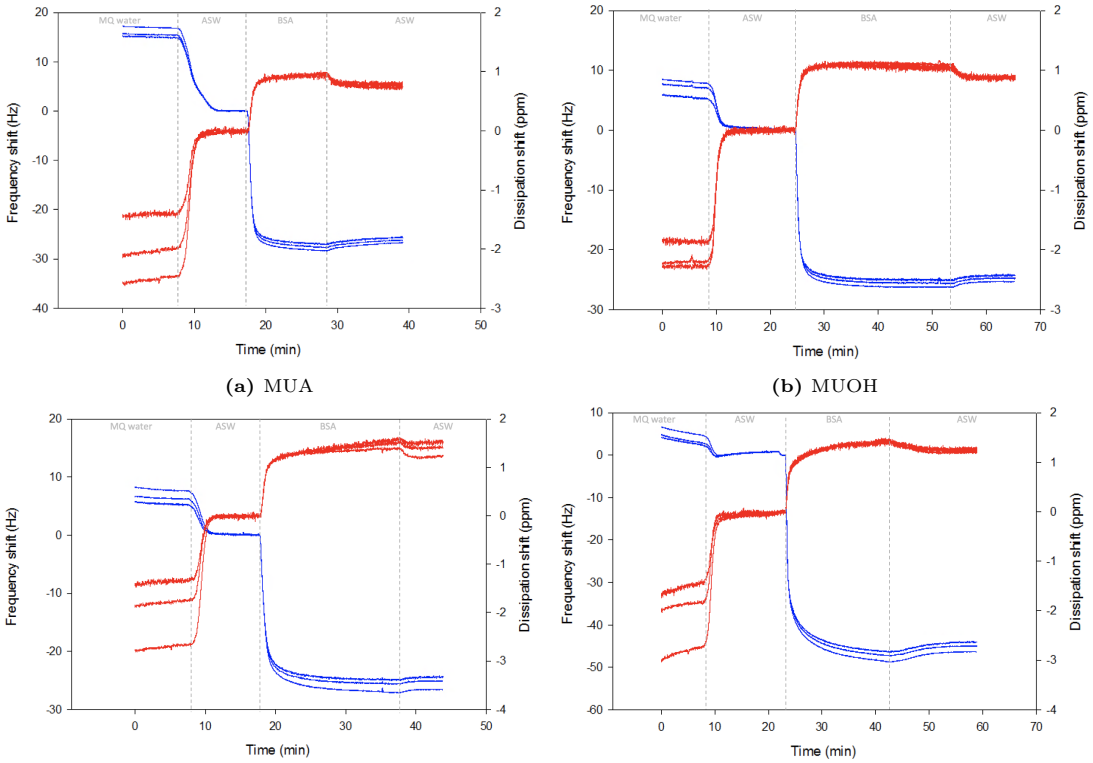

(a) MUA **(b)** MUOH

(c) DT10 **(d)** AUT

Figure 3.4: Frequency and dissipation diagrams of BSA adsorption on polymers. Blue and red graphs represent frequency and dissipation (overtones 3, 5 and 7), respectively.

The overtones observed on all surfaces exhibited a tight pattern, accompanied by a low dissipation shift, which indicates a rigid adsorbed layer. The overtones on the hydrophobic, neutral

DT10 appeared slightly more widely spread, and a higher dissipation shift was observed, compared to the hydrophilic, neutral MUOH. This suggests the formation of a more viscoelastic layer on the hydrophobic polymer, which would contradict literature. It is well-documented that proteins tend to adopt a smaller and more collapsed structure on hydrophobic surfaces due to the entropic penalty associated with water molecules being in close proximity to the surface, resulting in reduced hydration of the proteins. Conversely, hydrophilic surfaces promote protein swelling, as they provide a favorable environment for hydration.[50] It may however, be argued that the differences in frequency and dissipation are not significant. Given that the experiments were only performed once, this trend would likely decrease with more repetitions.

Lysozyme/BSA Adsorption

The frequency and dissipation measurements obtained from the mixed protein solutions demonstrated the highest degree of variation across the different surfaces, as illustrated in Figure 3.5. Frequency and dissipation curves from mixed protein solution encompass characteristics observed in the individual protein solution diagrams. Based solely on these diagrams, it appears that initial adsorption was driven by BSA. There are distinct similarities in the frequency drops observed after introducing the protein solution, which closely resemble the drops observed in pure BSA solutions as depicted in Figure 3.4. Further, the adsorption process continued beyond the initial stage, with a gradual decrease in slope over a prolonged period. This resembles the diagrams from lysozyme adsorption in Figure 3.3.

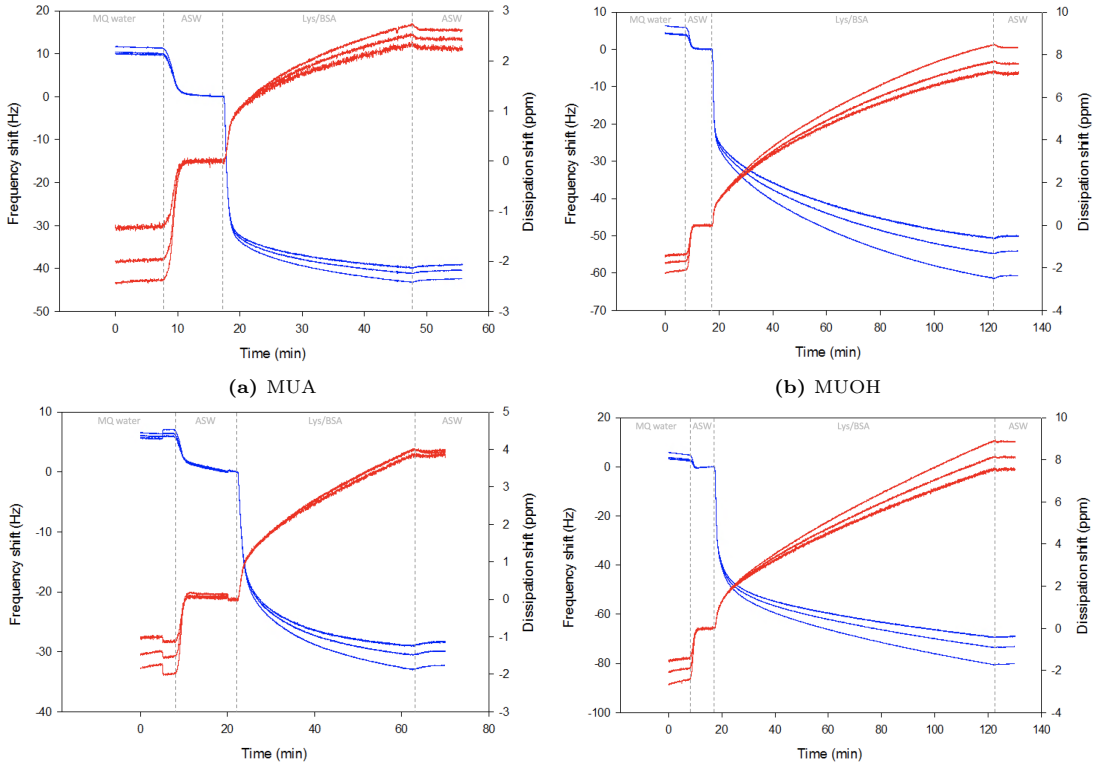

(a) MUA **(b)** MUOH

(c) DT10 **(d)** AUT

Figure 3.5: Frequency and dissipation diagrams of BSA/lysozyme adsorption on polymers. Blue and red graphs represent frequency and dissipation (overtones 3, 5 and 7), respectively.

Frequency decreased the most on AUT, suggesting that BSA had a more dominant role than lysozyme in the mixed solution. The frequency shift was greater for AUT than MUOH, but dissipation shifts were similar. This indicates formation of a more viscolastic layer on AUT.

3.3.2 Mass of Adsorbed Protein Layers

Mass of the adsorbed layer was estimated using models for viscoelastic layers in the Qsense Dfind software. It is important to note that both bound proteins and trapped associated water molecules cause the change in frequency and dissipation, meaning the approximated mass stems not only from bound protein.

Lysozyme

Estimated mass of the adsorbed layer is displayed in Figure 3.6. As suggested by the discussed frequency changes, there was significant mass on all surfaces. Areal mass of adsorbed lysozyme was around 4000 ng/cm^2 on the hydrophilic, uncharged MUOH, and closer to 5000 ng/cm^2 on the three other surfaces. Curve shapes are also relatively similar for MUA, DT10 and AUT, where there is a great increase in mass the first minutes before it gradually levels off. The shape of the MUOH curve, on the other hand, was different. Initial adsorption rate was lower was lower on this surface, which might be explained by a strong hydration layer on the surface and lack of electrostatic interactions between protein and polymer. Given that the surface is polar, there are likely ions adsorbed on the layer from ASW that promote adsorption. However, electrostatic interactions on MUA and AUT, and hydrophobic interactions on DT10, are likely stronger.

The curve of MUA starts to level out around 3000 ng/cm^2, while the same happens at a mass of 2000 ng/cm^2 for AUT. This indicates that initial lysozyme adsorption onto the oppositely charged surface was more favorable. However, adsorbed mass at the end of the experiment was similar on the two surfaces. One explanation for this is that only the first layer was directly dependent on the properties of the polymer layer, while the next layers adsorb onto the formed protein monolayer.

On all surfaces, mass decrease during rinsing was negligible. This indicates strong, irreversible binding of lysozyme.

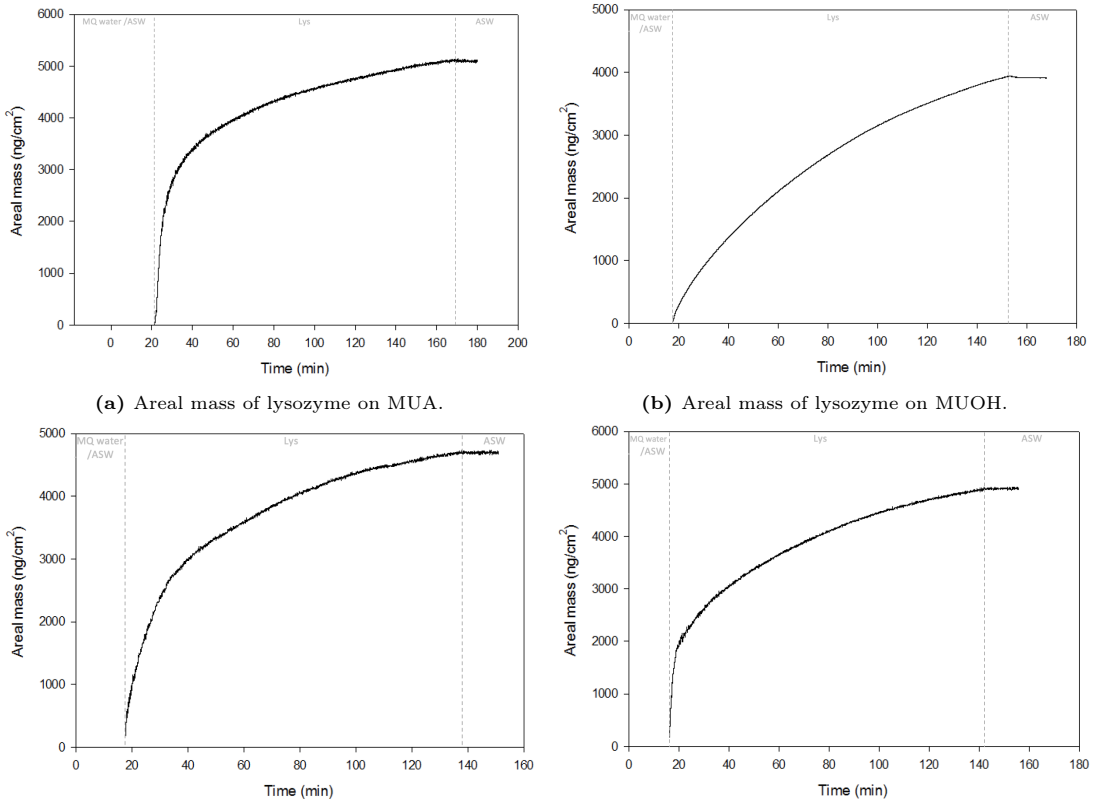

(a) Areal mass of lysozyme on MUA.

(b) Areal mass of lysozyme on MUOH.

(c) Areal mass of lysozyme on DT10.

(d) Areal mass of lysozyme on AUT.

Figure 3.6: Areal mass of adsorbed lysozyme on the four SAM surfaces detected by QCM-D.

BSA

For BSA, there was significantly more adsorption on the hydrophobic DT10 than all hydrophilic surfaces. While the mass quickly stabilized on the hydrophilic surfaces, it continued to increase on DT10. This indicates that hydrophobic interactions are the major driving force. It also indicates that the electrostatic interactions are less dominant in artificial seawater. This may be due to the ions shielding surface charges.

There was more adsorption of the negatively charged BSA on the positive AUT surface than the negative MUA surface, likely attributed to electrostatic attraction. The adsorption of a negatively charged protein onto a negatively charged surface may be explained by electrostatic interactions between positively charged domains in the protein and the surface. BSA contains the positively charged amino acids lysine and histidine.[9]

Mass decrease upon rinsing was significant for BSA, indicating weaker bonds than the ones formed by lysozyme. From literature, it would be expected that bonds were strong due to conformational changes and exposure of hydrophobic residues to the surface. The decrease in mass upon rinsing might stem from water dissociating from the adsorbed layer. Frequency and dissipation diagrams in Figure 3.4 support this hypothesis, since changes in dissipation relative to frequency was greater during the rinsing sequence than it was when proteins adsorbed to the surface. On AUT little mass was lost during rinsing, indicating stronger bonds, or possibly a less hydrated layer, of BSA on this surface than the other.

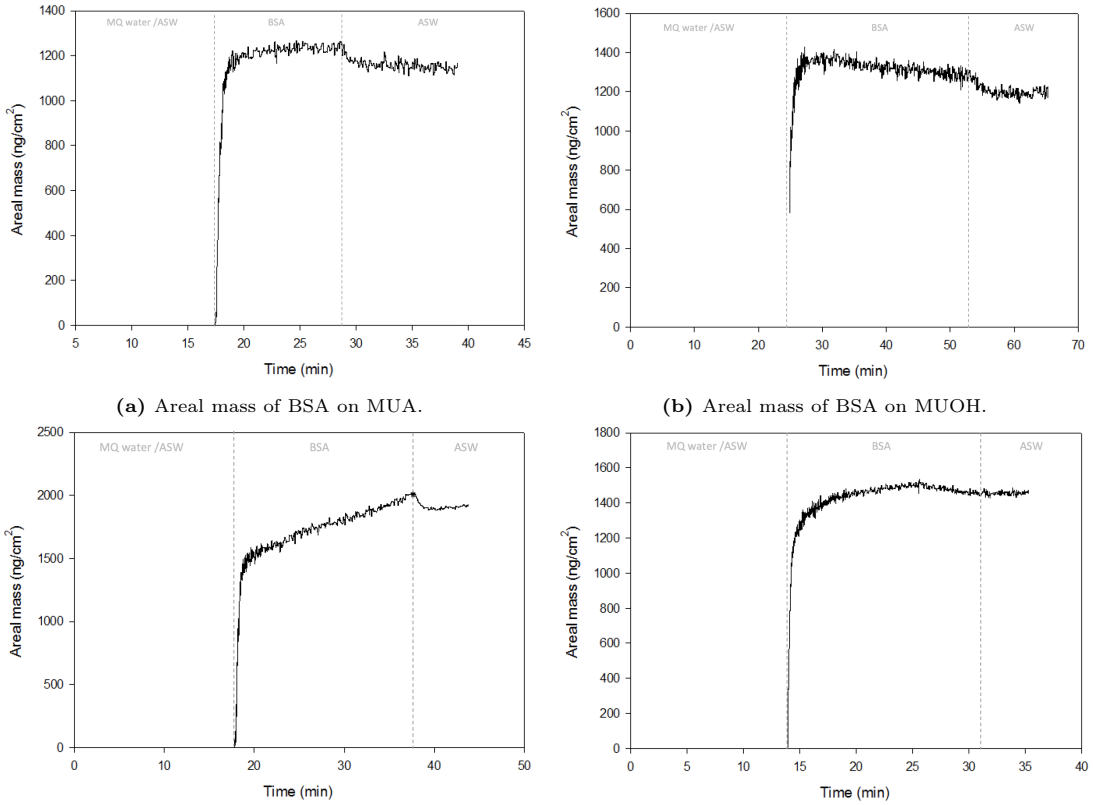

(a) Areal mass of BSA on MUA.

(b) Areal mass of BSA on MUOH.

(c) Areal mass of BSA on DT10.

(d) Areal mass of BSA on AUT.

Figure 3.7: Areal mass of adsorbed BSA on the four SAM surfaces detected by QCM-D.

Lysozyme/BSA

Even though the graphs in Figure 3.8 appear different at first, they all have a steep increase until the mass passes 1000 ng/cm^2 and the slope drastically decreases. This is similar to the initial period in the mass diagrams for BSA, suggesting that BSA adsorbs quickly to the surface immediately. However, graphs do not level off since lysozyme is likely adsorbed on top of the formed BSA monolayer.

It is noted that after the initial period of BSA adsorption, the graph of MUOH deviates from the other in the same way it did for pure lysozyme solution. This further supports the hypothesis of BSA adsorption followed by adsorption of lysozyme.

Lysozyme may have stronger affinity towards BSA or other lysozyme molecules than the surface. When the pH is between the pI of two oppositely charged proteins, they may form heteroprotein complexes. BSA contains active sites where lysozyme can bind. Lysozyme may also form intermolecular bonds with other lysozyme molecules. [46]

Upon rinsing, no mass was desorbed. This indicates strongly bound molecules. On DT10 and AUT the mass actually continued to increase during the ASW flushing, which may be due to association of more water molecules or ions.

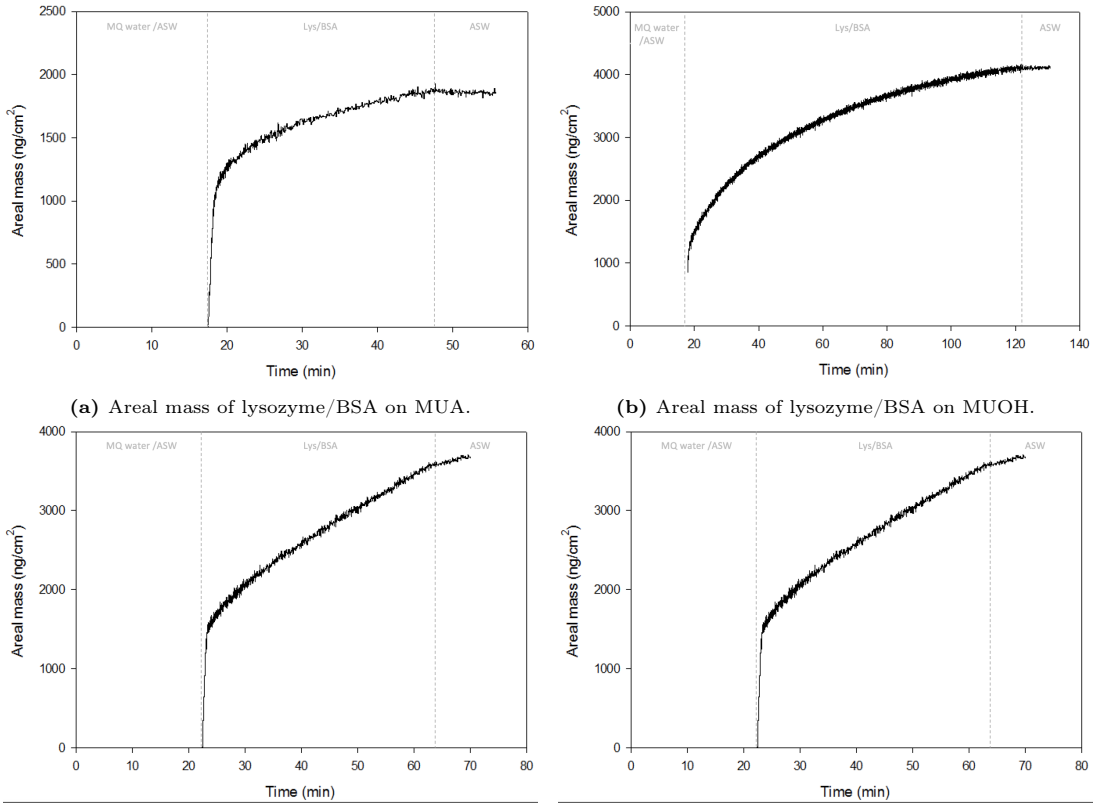

(a) Areal mass of lysozyme/BSA on MUA.

(b) Areal mass of lysozyme/BSA on MUOH.

(c) Areal mass of lysozyme/BSA on DT10.

(d) Areal mass of lysozyme/BSA on AUT.

Figure 3.8: Areal mass of adsorbed lysozyme/BSA on the four SAM surfaces detected by QCM-D.

3.3.3 Thickness of Adsorbed Protein Layers

Since all layers were assumed to have the same density (1100g/L), the thickness relations are similar to the ones of mass. The density assumption may have lead to bias in the estimated thickness. It should also be noted that the thickness is an estimated average, and deviations from theory might stem from defects in the formed SAMs or the gold sensors.

Since the mass detected by QCM-D is "wet mass" including coupled water molecules, number of layers cannot be determined by this technique alone. To estimate the number of layers, techniques such as surface plasmon resonance (SPR) that determine the dry mass could be used.

As can also be seen from the frequency and mass, there was significantly more adsorption of lysozyme than BSA on all surfaces. For lysozyme, it is difficult to estimate the number of layers based on the thickness determined by QCM-D. Dimensions of lysozyme are 4.5x3x3 nm. [5] As discussed previously, the high dissipation shifts indicate viscoelastic behavior and large amounts of associated water. However, comparing the dimensions of lysozyme to the thicknesses obtained of around 40 nm, multilayers are likely formed on all surfaces. Experiments were stopped before frequency and dissipation graphs were leveled off, meaning the thickness would have been higher if they were run longer. However, results are considered comparable since they were all stopped at the same threshold value.

The dimensions of BSA in aqueous solution is 4x4x14 nm. [9] Thickness of BSA was estimated to 12 nm on MUA and MUOH, 18 nm on DT10 and 14 nm on AUT. Since the thickness was higher than 4 nm, it is likely that BSA arranged in an end-on formation on all surfaces. A mono- or dilayer may also be formed in a side-on orientation, which would result in thicknesses of 4 or 8 nm, respectively. However, BSA typically forms monolayers on surfaces. The major

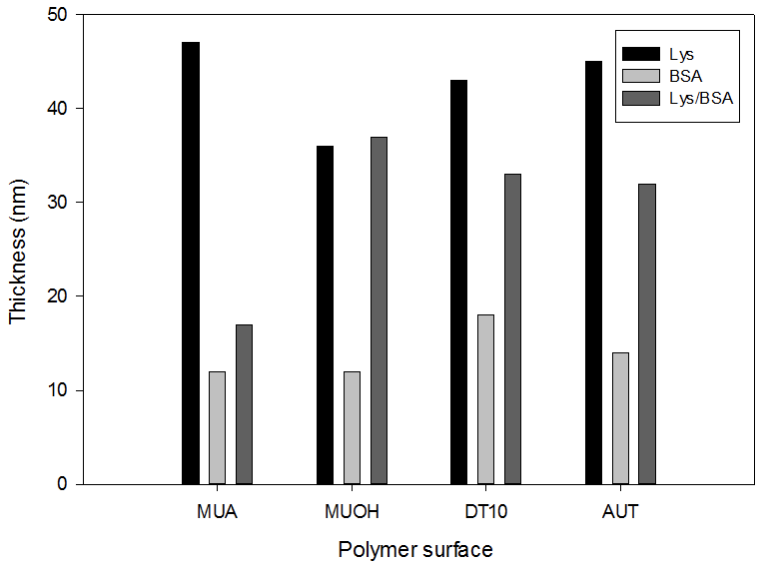

Figure 3.9: Calculated thickness of adsorbed protein layers on SAM surfaces.

difference between 12 and 4 nm can not be attributed to associated water, and it is therefore probable that the orientation is end-on on all surfaces. The monolayer may be incomplete due to defects in the polymer surface. Higher dissipation shift and more spread overtones indicating more viscoelastic properties on the hydrophobic DT10 suggests that the higher thickness may be attributed to coupled water molecules.

The thickness of BSA/lysozyme on MUA was significantly lower than on the other SAMs. It may be speculated that lysozyme formed complexes with BSA in solution before QCM-D measurements, meaning most proteins were bound in advance. Further experiments must be performed in order to fully understand interactions between lysozyme and BSA under these conditions.

3.3.4 Protein Adsorption Rate

Adsorption rate was determined by performing a slope analysis on the frequency of the 3rd overtone in all experiments. This was decided since the software occasionally failed to determine the mass at the beginning of the protein adsorption process, as can be seen in multiple figures. The adsorption rates may represent trends, but their absolute values are likely unreliable since they stem only from a single experiment. The lowest values resemble the highest adsorption rates, given mass increases when frequency decreases.

For all experiments, maximum adsorption rate was obtained shortly after the protein solutions were introduced. The rate was significantly higher for solutions containing BSA than lysozyme.

Table 3.3: Maximum adsorption rate of protein solutions on SAMs [mHz/s].

	MUA	MUOH	DT10	AUT
Lys	-2.0	-3.8	-7.8	-1.75
BSA	-13.8	-11.5	-10.0	-22.5
Lys/BSA	-16.3	-12.8	-6.0	-17.3

For BSA, maximum adsorption rate was significantly higher on the oppositely charged AUT than all other surfaces. Second highest was MUA, which indicates that electrostatic interactions were a strong driving force in the initial phase.

Contrary to pure lysozyme solution and similarly to BSA, the mixed solution exhibited the highest rate on the charged surfaces. This further strengthens the hypothesis where BSA adsorbs firstly on all surfaces.

3.3.5 Phase Analysis

To better understand the kinetics of the adsorption process, frequency and dissipation shifts were compared. Plotting $\Delta D/\Delta F$ for the adsorption makes it possible to determine if it is a single- or multi-phase process. Number of different slopes indicates number of steps in the adsorption process.[80] Plots for lysozyme, BSA and lysozyme/BSA mix is displayed in Figure 3.10. Δ D/Δ F diagrams for adsorption on the other polymers studied were similar to the ones of MUOH, and can be found in Appendix A.4.

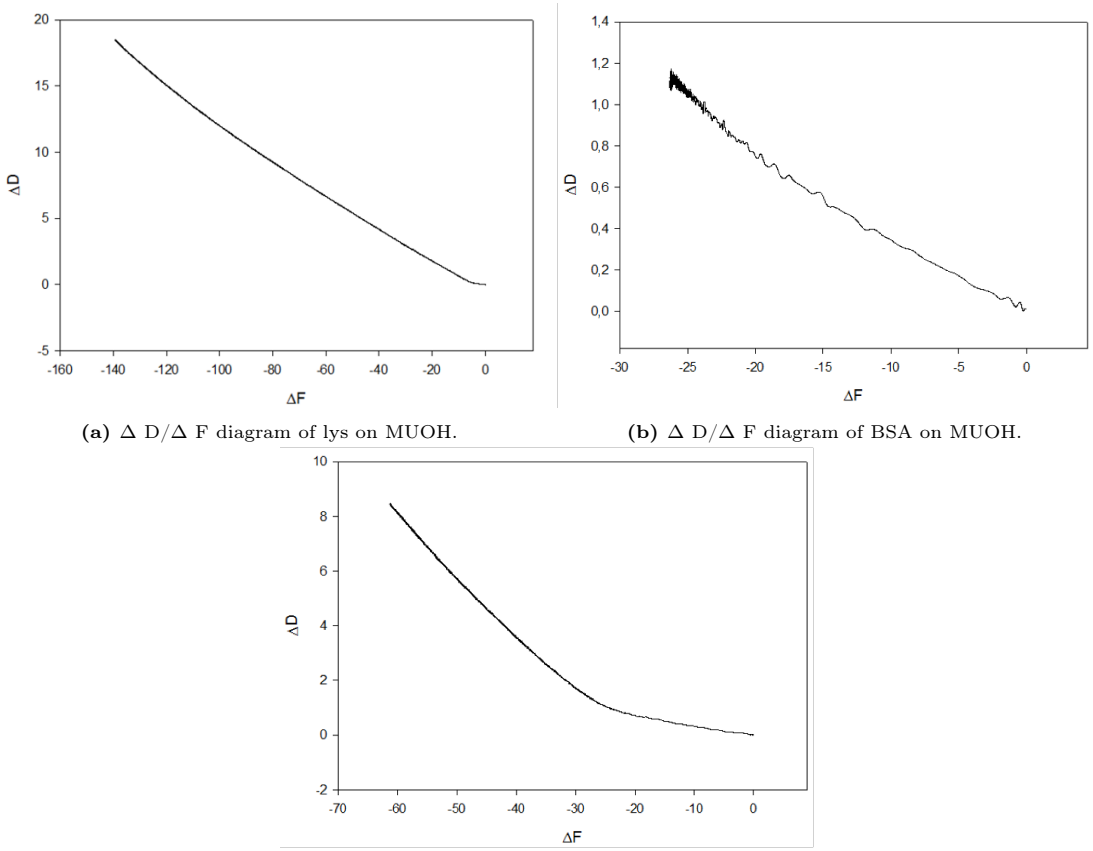

(a) Δ D/Δ F diagram of lys on MUOH.

(b) Δ D/Δ F diagram of BSA on MUOH.

(c) Δ D/Δ F diagram of lys/BSA on MUOH.

Figure 3.10: Layer softness per mass during protein adsorption on MUOH surface.

The relatively linear graph for lysozyme indicates that the adsorption process consists of a single step. Changes in frequency were likely caused by adsorption, and not by conformational changes on the surface.

For BSA, the graph is also sufficiently linear to suggest a single-step process. The deviation from a straight line might be explained by the adsorption rate, where all of the adsorption happened within a small time scale and exhibiting more unstable signals than a slow process.

For the lysozyme/BSA mix, there are two distinct slopes indicating a two-step adsorption process. This is in agreement with the Vroman effect described in literature, where small molecules adsorb first but are displaced by larger molecules. However, as discussed previously, BSA likely adsorbed first. In the frequency interval between 0 and -25 in Figure 3.10 dissipation

shift was low, which further supports this hypothesis. As discussed previously, this is likely attributed to high surface affinity of BSA.

3.3.6 Effect of Lysozyme Concentration on Adsorption

To investigate the influence of concentration, sequential depositions of lysozyme were conducted on the four surfaces. The estimated mass data is illustrated in Figure 3.11. Notably, the hydrophobic surface exhibited the highest mass, suggesting that hydrophobic forces played a significant role in the adsorption process. While the variations in adsorbed mass are discussed, it is essential to acknowledge that substantial masses were detected on all surfaces. Specifically, the order of increasing mass adsorption during sequential depositions was AUT $<$ MUOH $<$ MUA $<$ DT10. The surface with a similar charge as the lysozyme, AUT, exhibited the least adsorption.

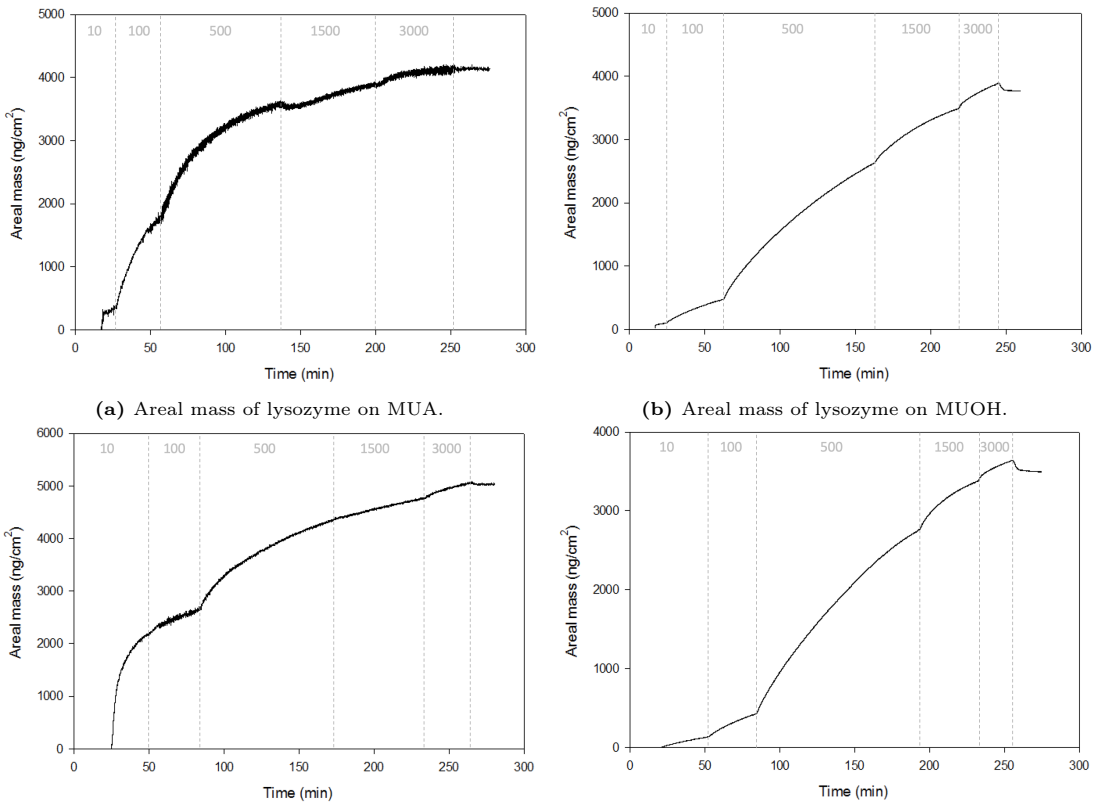

(a) Areal mass of lysozyme on MUA.

(b) Areal mass of lysozyme on MUOH.

(c) Areal mass of lysozyme on DT10.

(d) Areal mass of lysozyme on AUT.

Figure 3.11: Areal mass of adsorbed lysozyme on the four SAM surfaces during sequential deposition.

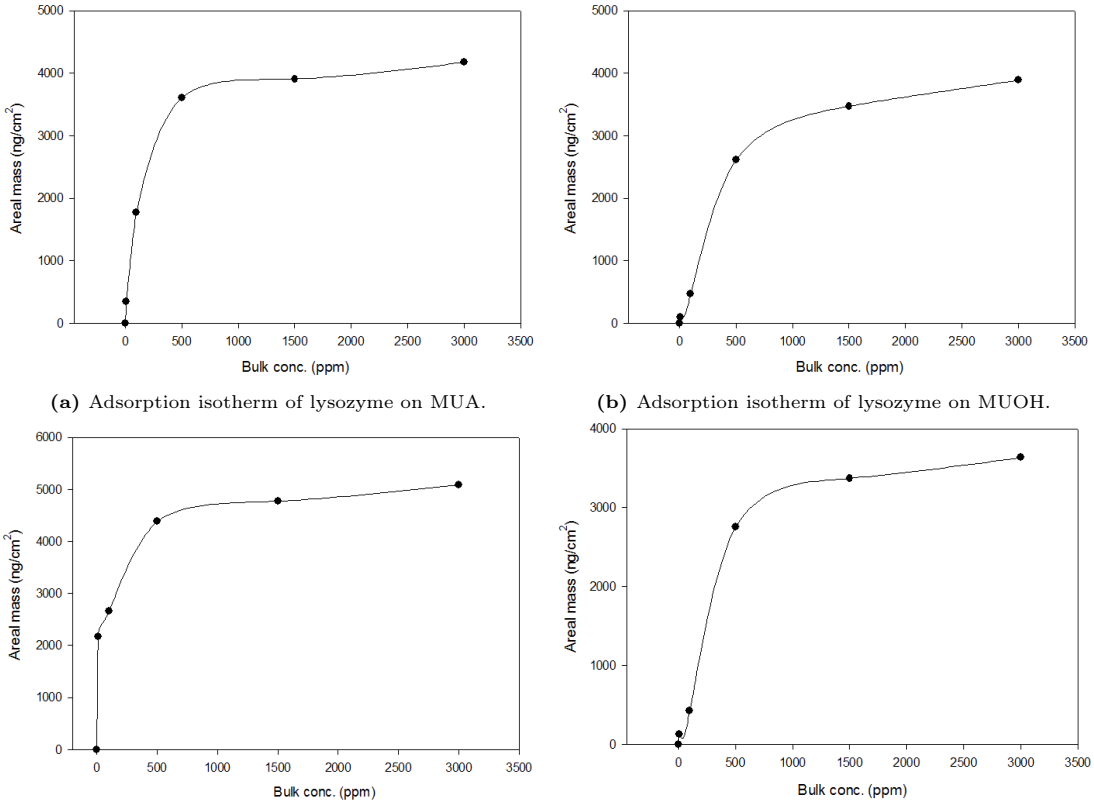

(a) Adsorption isotherm of lysozyme on MUA.

(b) Adsorption isotherm of lysozyme on MUOH.

(c) Adsorption isotherm of lysozyme on DT10.

(d) Adsorption isotherm of lysozyme on AUT.

Figure 3.12: Adsorption isotherms of 10, 100, 500, 1500 and 3000 ppm lysozyme on the four SAM surfaces during sequential deposition.

The shape of the isotherm plots in Figure 3.12 fit the characteristic shape of a Langmuir isotherm. They may also resemble the shape of the Freundlich isotherm, considering the graphs don't completely level off. However, both of these models are based on assumptions of monolayer formation. As discussed previously, multilayers are likely formed on all surfaces. The BET isotherm provides for multilayer adsorption, but the typical shape is not similar to any of the ones produced in this study. The results indicate that maximum adsorption was almost reached at a solution concentration of 500 ppm lysozyme.

A maximum slope analysis was performed on the 3rd overtone of the frequency diagrams from the sequential depositions. The highest adsorption rate was obtained shortly after the solution was introduced for all concentrations. The frequency shift was greatest for the first lysozyme solution (10 ppm), except on AUT. This might be due to initial electrostatic repulsion between similarly charged surfaces. Lysozyme on MUOH also exhibited the lowest rate of the single concentration experiments. For the higher concentrations, maximum adsorption rates were more similar.

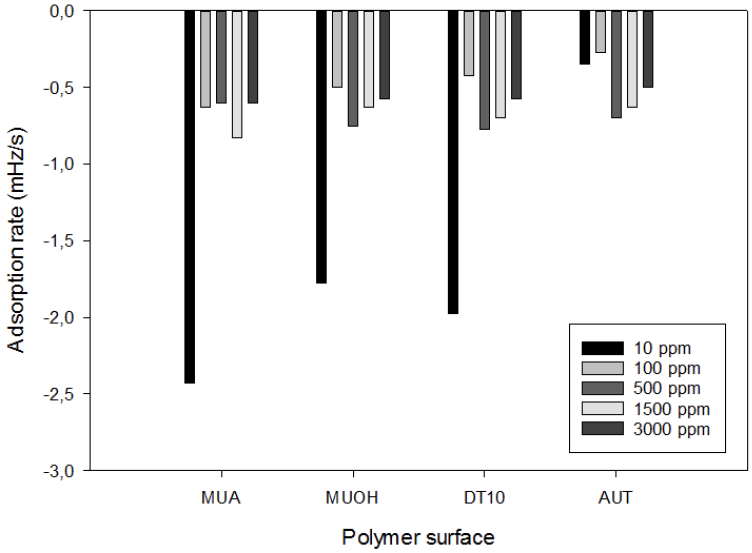

Figure 3.13: Maximal adsorption rate of different lysozyme concentrations on MUA, MUOH, DT10 and AUT.

On all other surfaces than MUA, lowest adsorption rate was obtained for 100 ppm solution. 500 ppm exhibited the second highest adsorption rate, while it decreased slightly with increasing concentration. Since new solutions were introduced before equilibrium was reached, the effect of increase in concentration above 500 ppm was likely minimal.

4 Conclusion

Marine biofouling remains a huge challenge for multiple marine sectors. This project was focused around hydrophobic and hydrophilic surfaces, while also investigating impacts of charges on the surface. The adsorption mechanisms of two proteins on different polymer surfaces was probed using QCM-D.

Investigating protein adsprotion processes is a complex endeavor. Similar with previous literature, none of the surfaces studied were protein resistant. The adsorption kinetics of lysozyme and BSA greatly differed. While lysozyme adsorption continued for hours, the majority of BSA was adsorbed after seconds to minutes. Hence, BSA adsorption was a quicker process.

Despite the smaller relative size of lysozyme, thickness and mass of adsorbed lysozyme was larger in all experiments. Based on the thickness, BSA likely formed a monolayer on all surfaces. Lysozyme, on the other hand, likely formed multilayers. This indicates favorable intermolecular interactions between lysozyme molecules. In the case of multilayer formation, only adsorption of the first layer is directly dependent on the surface properties.

Both lysozyme and BSA adsorption are believed to be single-phase processes. When the two were mixed, however, results indicated two phases. The first phase was likely BSA adsorption, while lysozyme adsorbed at a later stage. This order is opposite to the Vroman effect, which describes adsorption of smaller molecules first. The reason for this is unknown. Whether lysozyme molecules displace BSA or adsorb on top is also unknown.

Ionic strength of the seawater appears to be of high significance for protein adsorption processes. Surface charge seems to be less significant in systems with higher ionic strength, such as the one studied in this project. This is attributed to formation of an electric double layer of ions on the surface. In the context of marine biofouling, where ionic strength varies in different geographical locations, it is important to notice the large impact of this factor.

5 Future Work

As previously highlighted, QCM-D experiments were performed only once. Given the variability in reproducibility observed in literature, the subsequent crucial step would involve replicating these experiments to assess the reliability of the results. This would also provide a better indication of how successful the SAM formation was, since good reproducibility would suggest a complete monolayer.

By comparing data from QCM-D and multi-parameter surface plasmon resonance (MP-SPR), the hydration, and number, of adsorbed protein layers can be determined.[81] Spectroscopic ellipsometry (SE) could also be used for this purpose.[9]

The influence of ionic strength on the adsorption behavior of proteins on surfaces is evidently significant. Therefore, it is highly recommended to investigate the impact of varying ionic strengths on the adsorption processes. The obtained results of BSA adsorption in this particular study exhibited substantial deviations from the existing literature, which can likely be attributed to the elevated ionic strength and the subsequent formation of an electrical double layer on the surfaces.

Additionally, I would propose conducting protein adsorption studies on both hydrophobic and hydrophilic surfaces commonly employed in the industry.

References

[1] H. Y. Qiu, K. Feng, A. Gapeeva, K. Meurisch, S. Kaps, X. Li, L. M. Yu, Y. K. Mishra, R. Adelung, and M. Baum. Functional polymer materials for modern marine biofouling control. *Progress in Polymer Science*, 127, 2022. ISSN 0079-6700. doi: ARTN10151610.1016/j.progpolymsci.2022.101516. URL <GotoISI>://WOS:000820174200003.

[2] URL https://www.sigmaaldrich.com/NO/en/product/aldrich/81260.

[3] H. Yang, R. Wen, H. Zhao, M. Guo, L. Zhang, and Y. Chen. Study on ageing characteristics and evaluation methods of rtv silicone rubber in high humidity area. *Plos One*, 16(6), 2021. ISSN 1932-6203. doi: ARTNe025109210.1371/journal.pone.0251092. URL <GotoISI>://WOS:000664640100013.

[4] H. Zhang and M. Chiao. Anti-fouling coatings of poly(dimethylsiloxane) devices for biological and biomedical applications. *J Med Biol Eng*, 35(2):143–155, 2015. ISSN 1609-0985 (Print) 2199-4757 (Electronic) 1609-0985 (Linking). doi: 10.1007/s40846-015-0029-4. URL https://www.ncbi.nlm.nih.gov/pubmed/25960703.

[5] P. Komorek, M. Walek, and B. Jachimska. Mechanism of lysozyme adsorption onto gold surface determined by quartz crystal microbalance and surface plasmon resonance. *Bioelectrochemistry*, 135, 2020. ISSN 1567-5394. doi: ARTN10758210.1016/j.bioelechem.2020.107582. URL <GotoISI>://WOS:000579730600025.

[6] R. A. Latour. The langmuir isotherm: A commonly applied but misleading approach for the analysis of protein adsorption behavior. *Journal of Biomedical Materials Research Part A*, 103(3):949–958, 2015. ISSN 1549-3296. doi: 10.1002/jbm.a.35235. URL <GotoISI>://WOS:000349103500010.

[7] J. C. Love, L. A. Estroff, J. K. Kriebel, R. G. Nuzzo, and G. M. Whitesides. Self-assembled monolayers of thiolates on metals as a form of nanotechnology. *Chemical Reviews*, 105 (4):1103–1169, 2005. ISSN 0009-2665. doi: 10.1021/cr0300789. URL <GotoISI>://WOS:000228412800003.

[8] Qcm-d measurement. 2022. URL https://www.biolinscientific.com/measurements/qcm-d.

[9] H. T. M. Phan, S. Bartelt-Hunt, K. B. Rodenhausen, M. Schubert, and J. C. Bartz. Investigation of bovine serum albumin (bsa) attachment onto self-assembled monolayers (sams) using combinatorial quartz crystal microbalance with dissipation (qcm-d) and spectroscopic ellipsometry (se). *Plos One*, 10(10), 2015. ISSN 1932-6203. doi: ARTNe014128210.1371/journal.pone.0141282. URL <GotoISI>://WOS:000363804200042.

[10] G. B. Sigal, M. Mrksich, and G. M. Whitesides. Effect of surface wettability on the adsorption of proteins and detergents. *Journal of the American Chemical Society*, 120 (14):3464–3473, 1998. ISSN 0002-7863. doi: DOI10.1021/ja970819l. URL <GotoISI>://WOS:000073179200024.

[11] R. Rayner, C. Jolly, and C. Gouldman. Ocean observing and the blue economy. *Frontiers in Marine Science*, 6, 2019. doi: ARTN33010.3389/fmars.2019.00330. URL <GotoISI>://WOS:000471698800001.

[12] L. Vedaprakash, P. Senthilkumar, D. Inbakandan, and R. Venkatesan. *Marine Biofouling and Corrosion on Long-Term Behavior of Marine Structures*. Indian Institute of Metals Series. Springer, Singapore, 2022. doi: 10.1007/978-981-16-9302-1_24.

[13] I. Amara, W. Miled, R. Ben Slama, and N. Ladhari. Antifouling processes and toxicity effects of antifouling paints on marine environment. a review. *Environmental Toxicology*

and Pharmacology, 57:115–130, 2018. ISSN 1382-6689. doi: 10.1016/j.etap.2017.12.001. URL <GotoISI>://WOS:000425199400015.

[14] A. Rosenhahn, S. Schilp, H. J. Kreuzer, and M. Grunze. The role of "inert" surface chemistry in marine biofouling prevention. *Physical Chemistry Chemical Physics*, 12(17): 4275–4286, 2010. ISSN 1463-9076. doi: 10.1039/c001968m. URL <GotoISI>://WOS:000276896000002.

[15] G. Galli and E. Martinelli. Amphiphilic polymer platforms: Surface engineering of films for marine antibiofouling. *Macromolecular Rapid Communications*, 38(8), 2017. ISSN 1022-1336. doi: ARTN160070410.1002/marc.201600704. URL <GotoISI>://WOS:000400377600002.

[16] W. F. Yang, R. Zhang, Y. Wu, X. W. Pei, Y. P. Liu, and F. Zhou. Enhancement of graft density and chain length of hydrophilic polymer brush for effective marine antifouling. *Journal of Applied Polymer Science*, 135(22), 2018. ISSN 0021-8995. doi: ARTN4623210.1002/app.46232. URL <GotoISI>://WOS:000426508700003.

[17] M. Rabe, D. Verdes, and S. Seeger. Understanding protein adsorption phenomena at solid surfaces. *Advances in Colloid and Interface Science*, 162(1-2):87–106, 2011. ISSN 0001-8686. doi: 10.1016/j.cis.2010.12.007. URL <GotoISI>://WOS:000288638400007.

[18] G. B. Yu, J. Liu, and J. Zhou. Mesoscopic coarse-grained simulations of lysozyme adsorption. *Journal of Physical Chemistry B*, 118(17):4451–4460, 2014. ISSN 1520-6106. doi: 10.1021/jp409326f. URL <GotoISI>://WOS:000335433000001.

[19] L. Telegdi, L. Trif, and L. Románski. *Smart anti-biofouling composite coatings for naval applications*, book section 5. Elsevier Ltd, 5th edition, 2016.

[20] P. A. Vinagre, T. Simas, E. Cruz, E. Pinori, and J. Svenson. Marine biofouling: A european database for the marine renewable energy sector. *Journal of Marine Science and Engineering*, 8(7), 2020. doi: ARTN49510.3390/jmse8070495. URL <GotoISI>://WOS:000556382400001.

[21] S. J. Lin, H. C. Bi, C. E. Weinell, and K. Dam-Johansen. Submerged surfaces exposed to marine biofouling - experimental investigation of cleaning parameters effectiveness (vol 172, 107097, 2022). *Progress in Organic Coatings*, 173, 2022. ISSN 0300-9440. doi: ARTN10722910.1016/j.porgcoat.2022.107229. URL <GotoISI>://WOS:000871100000007.

[22] B. E. T. Bautista, M. L. Carvalho, A. Seyeux, S. Zanna, P. Cristiani, B. Tribollet, P. Marcus, and I. Frateur. Effect of protein adsorption on the corrosion behavior of 70cu-30ni alloy in artificial seawater. *Bioelectrochemistry*, 97:34–42, 2014. ISSN 1567-5394. doi: 10.1016/j.bioelechem.2013.10.004. URL <GotoISI>://WOS:000334083300006.

[23] K. Zecher, V. P. Aitha, K. Heuer, H. Ahlers, K. Roland, M. Fiedel, and B. Philipp. A multi-step approach for testing non-toxic amphiphilic antifouling coatings against marine microfouling at different levels of biological complexity. *Journal of Microbiological Methods*, 146:104–114, 2018. ISSN 0167-7012. doi: 10.1016/j.mimet.2018.02.009. URL <GotoISI>://WOS:000428490300021.

[24] J. A. Callow and M. E. Callow. Trends in the development of environmentally friendly fouling-resistant marine coatings. *Nature Communications*, 2, 2011. ISSN 2041-1723. doi: ARTN24410.1038/ncomms1251. URL <GotoISI>://WOS:000289982600034.

[25] W. Yandi, S. Mieszkin, A. di Fino, P. Martin-Tanchereau, M. E. Callow, J. A. Callow, L. Tyson, A. S. Clare, and T. Ederth. Charged hydrophilic polymer brushes and their relevance for understanding marine biofouling. *Biofouling*, 32(6):609–625, 2016. ISSN 0892-7014. doi: 10.1080/08927014.2016.1170816. URL <GotoISI>://WOS:000377117900001.

[26] I. C. Nwuzor, C. I. Idumah, S. C. Nwanonenyi, and O. E. Ezeani. Emerging trends in self-polishing anti-fouling coatings for marine environment. *Safety in Extreme Environments*, 3:9–25, 2021. doi: 0.1007/s42797-021-00031-3.

[27] S. Kaur, I. M. Kempson, J. B. Linden, M. Larsson, and M. Nyden. Unhindered copper uptake by glutaraldehyde-polyethyleneimine coatings in an artificial seawater model system with adsorbed swollen polysaccharides and competing ligand edta. *Biofouling*, 33(2):184–194, 2017. ISSN 0892-7014. doi: 10.1080/08927014.2017.1284204. URL <GotoISI>://WOS:000395114700006.

[28] A. M. C. Maan, A. H. Hofman, W. M. de Vos, and M. Kamperman. Recent developments and practical feasibility of polymer-based antifouling coatings. *Advanced Functional Materials*, 30(32), 2020. ISSN 1616-301x. doi: ARTN200093610.1002/adfm.202000936. URL <GotoISI>://WOS:000536853100001.

[29] K. Y. Law. Definitions for hydrophilicity, hydrophobicity, and superhydrophobicity: Getting the basics right. *Journal of Physical Chemistry Letters*, 5(4):686–688, 2014. ISSN 1948-7185. doi: 10.1021/jz402762h. URL <GotoISI>://WOS:000331860900008.

[30] W. Yandi, S. Mieszkin, P. Martin-Tanchereau, M. E. Callow, J. A. Callow, L. Tyson, B. Liedberg, and T. Ederth. Hydration and chain entanglement determines the optimum thickness of poly(hema-co-peg(10)ma) brushes for effective resistance to settlement and adhesion of marine fouling organisms. *Acs Applied Materials & Interfaces*, 6(14): 11448–11458, 2014. ISSN 1944-8244. doi: 10.1021/am502084x. URL <GotoISI>://WOS:000339472100078.

[31] A. Larsson, T. Ekblad, O. Andersson, and B. Liedberg. Photografted poly(ethylene glycol) matrix for affinity interaction studies. *Biomacromolecules*, 8(1):287–295, 2007. ISSN 1525-7797. doi: 10.1021/bm060685g. URL <GotoISI>://WOS:000243337600039.

[32] T. Ekblad, G. Bergstroem, T. Ederth, S. L. Conlan, R. Mutton, A. S. Clare, S. Wang, Y. L. Liu, Q. Zhao, F. D'Souza, G. T. Donnelly, P. R. Willemsen, M. E. Pettitt, M. E. Callow, J. A. Callow, and B. Liedberg. Poly(ethylene glycol)-containing hydrogel surfaces for antifouling applications in marine and freshwater environments. *Biomacromolecules*, 9(10):2775–2783, 2008. ISSN 1525-7797. doi: 10.1021/bm800547m. URL <GotoISI>://WOS:000260049500030.

[33] L. C. Zheng, H. S. Sundaram, Z. Y. Wei, C. C. Li, and Z. F. Yuan. Applications of zwitterionic polymers. *Reactive and Functional Polymers*, 118:51–61, 2017. ISSN 1381-5148. doi: 10.1016/j.reactfunctpolym.2017.07.006. URL <GotoISI>://WOS:000408786800007.

[34] I. Jimenez-Pardo, L. G. J. van der Ven, R. A. T. M. van Benthem, G. de With, and A. C. C. Esteves. Hydrophilic self-replenishing coatings with long-term water stability for anti-fouling applications. *Coatings*, 8(5), 2018. ISSN 2079-6412. doi: ARTN18410.3390/coatings8050184. URL <GotoISI>://WOS:000435192400033.

[35] Y. Yang, H. L. Luo, J. L. Yang, D. F. Huang, and S. X. Zhou. Facile uv-curing technique to establish a 3d-grafted poly(ethylene glycol) layer on an epoxy resin base for underwater applications. *Journal of Applied Polymer Science*, 133(39), 2016. ISSN 0021-8995. doi: ARTN4397210.1002/app.43972. URL <GotoISI>://WOS:000380006000011.

[36] X. Su, D. Z. Hao, Z. N. Li, X. L. Guo, and L. Jiang. Design of hierarchical comb hydrophilic polymer brush (hchpb) surfaces inspired by fish mucus for anti-biofouling. *Journal of Materials Chemistry B*, 7(8):1322–1332, 2019. ISSN 2050-750x. doi: 10.1039/c8tb03278e. URL <GotoISI>://WOS:000459478600012.

[37] E. Martinelli, D. Gunes, B. M. Wenning, C. K. Ober, J. A. Finlay, M. E. Callow, J. A. Callow, A. Di Fino, A. S. Clare, and G. Galli. Effects of surface-active block copolymers with oxyethylene and fluoroalkyl side chains on the antifouling per-

formance of silicone-based films. *Biofouling*, 32(1):81–93, 2016. ISSN 0892-7014. doi: 10.1080/08927014.2015.1131822. URL <GotoISI>://WOS:000368561300009.

[38] Z. W. Lu, Z. Chen, Y. Guo, Y. Y. Ju, Y. Liu, R. Feng, C. X. Xiong, C. K. Ober, and L. J. Dong. Flexible hydrophobic antifouling coating with oriented nanotopography and nonleaking capsaicin. *Acs Applied Materials & Interfaces*, 10(11):9718–9726, 2018. ISSN 1944-8244. doi: 10.1021/acsami.7b19436. URL <GotoISI>://WOS:000428356800061.

[39] Y. Sun, Y. B. Ji, Y. H. Lang, L. Wang, B. Liu, and Z. Z. Zhang. A comparative study on the impact of the carbon nanotubes-modified polydimethylsiloxane nanocomposites on the colonization dynamics of the pioneer biofilm communities. *International Biodeterioration & Biodegradation*, 129:195–201, 2018. ISSN 0964-8305. doi: 10.1016/j.ibiod.2018.02.011. URL <GotoISI>://WOS:000429761000025.

[40] S. Tian, D. Y. Jiang, J. B. Pu, X. F. Sun, Z. M. Li, B. Wu, W. R. Zheng, W. Q. Liu, and Z. X. Liu. A new hybrid silicone-based antifouling coating with nanocomposite hydrogel for durable antifouling properties. *Chemical Engineering Journal*, 370:1–9, 2019. ISSN 1385-8947. doi: 10.1016/j.cej.2019.03.185. URL <GotoISI>://WOS:000467387200001.

[41] H. Y. Qiu, A. Gapeeva, I. Holken, S. Kaps, R. Adelung, and M. J. Baum. Polydimethylsiloxane microdomains formation at the polythiourethane/air interface and its influence on barnacle release. *Acs Applied Materials & Interfaces*, 13(3):4545–4552, 2021. ISSN 1944-8244. doi: 10.1021/acsami.0c20058. URL <GotoISI>://WOS:000614062400101.

[42] C. Liu, C. F. Ma, Q. Y. Xie, and G. Z. Zhang. Self-repairing silicone coatings for marine anti-biofouling. *Journal of Materials Chemistry A*, 5(30):15855–15861, 2017. ISSN 2050-7488. doi: 10.1039/c7ta05241c. URL <GotoISI>://WOS:000406672400043.

[43] C. Liu, Q. Y. Xie, C. F. Ma, and G. Z. Zhang. Fouling release property of polydimethylsiloxane-based polyurea with improved adhesion to substrate. *Industrial & Engineering Chemistry Research*, 55(23):6671–6676, 2016. ISSN 0888-5885. doi: 10.1021/acs.iecr.6b01003. URL <GotoISI>://WOS:000378194200013.

[44] H. Y. Qiu, I. Holken, A. Gapeeva, V. Filiz, R. Adelung, and M. Baum. Development and characterization of mechanically durable silicone-polythiourethane composites modified with tetrapodal shaped zno particles for the potential application as fouling-release coating in the marine sector. *Materials*, 11(12), 2018. doi: ARTN241310.3390/ma11122413. URL <GotoISI>://WOS:000456419200071.

[45] R. A. Latour. Fundamental principles of the thermodynamics and kinetics of protein adsorption to material surfaces. *Colloids and Surfaces B-Biointerfaces*, 191, 2020. ISSN 0927-7765. doi: ARTN11099210.1016/j.colsurfb.2020.110992. URL <GotoISI>://WOS:000535696800021.

[46] R. J. Sarmah and S. Kundu. Structure and morphology of bovine serum albumin-lysozyme (bsa-lys) complex films at air-water interface. *Food Hydrocolloids*, 131, 2022. ISSN 0268-005x. doi: ARTN10778810.1016/j.foodhyd.2022.107788. URL <GotoISI>://WOS:000817967300005.

[47] J. Kim and G. A. Somorjai. Molecular packing of lysozyme, fibrinogen, and bovine serum albumin on hydrophilic and hydrophobic surfaces studied by infrared-visible sum frequency generation and fluorescence microscopy. *Journal of the American Chemical Society*, 125 (10):3150–3158, 2003. ISSN 0002-7863. doi: 10.1021/ja028987n. URL <GotoISI>://WOS:000181409500063.

[48] M. Yang, C. Dutta, and A. Tiwari. Disulfide-bond scrambling promotes amorphous aggregates in lysozyme and bovine serum albumin. *Journal of Physical Chemistry B*, 119(10):3969–3981, 2015. ISSN 1520-6106. doi: 10.1021/acs.jpcb.5b00144. URL <GotoISI>://WOS:000351188300010.

[49] R. Swaminathan, V. K. Ravi, S. Kumar, M. V. S. Kumar, and N. Chandra. Lysozyme: A model protein for amyloid research. *Advances in Protein Chemistry and Structural Biology, Vol 84*, 84:63–111, 2011. ISSN 1876-1623. doi: 10.1016/B978-0-12-386483-3.00003-3. URL <GotoISI>://WOS:000294690100003.

[50] A. R. Hall and M. Geoghegan. Polymers and biopolymers at interfaces. *Reports on Progress in Physics*, 81(3), 2018. ISSN 0034-4885. doi: ARTN03660110.1088/1361-6633/aa9e9c. URL <GotoISI>://WOS:000423376500001.

[51] Z. Adamczyk. Protein adsorption: A quest for a universal mechanism. *Current Opinion in Colloid & Interface Science*, 41:50–65, 2019. ISSN 1359-0294. doi: 10.1016/j.cocis.2018.11.004. URL <GotoISI>://WOS:000472990600006.

[52] J. Malmstrom, H. Agheli, P. Kingshott, and D. S. Sutherland. Viscoelastic modeling of highly hydrated laminin layers at homogeneous and nanostructured surfaces: Quantification of protein layer properties using qcm-d and spr. *Langmuir*, 23(19):9760–9768, 2007. ISSN 0743-7463. doi: 10.1021/la701233y. URL <GotoISI>://WOS:000249241300037.

[53] H. Noh and E. A. Vogler. Volumetric interpretation of protein adsorption: Competition from mixtures and the vroman effect. *Biomaterials*, 28(3):405–422, 2007. ISSN 0142-9612. doi: 10.1016/j.biomaterials.2006.09.006. URL <GotoISI>://WOS:000242960900005.

[54] S. L. Hirsh, D. R. McKenzie, N. J. Nosworthy, J. A. Denman, O. U. Sezerman, and M. M. M. Bilek. The vroman effect: Competitive protein exchange with dynamic multilayer protein aggregates. *Colloids and Surfaces B-Biointerfaces*, 103:395–404, 2013. ISSN 0927-7765. doi: 10.1016/j.colsurfb.2012.10.039. URL <GotoISI>://WOS:000315127000052.

[55] L. Heinrich, E. K. Mann, J. C. Voegel, G. J. M. Koper, and P. Schaaf. Scanning angle reflectometry study of the structure of antigen-antibody layers adsorbed on silica surfaces. *Langmuir*, 12(20):4857–4865, 1996. ISSN 0743-7463. doi: DOI10.1021/la9602630. URL <GotoISI>://WOS:A1996VL05900036.

[56] P. Gupta, A. Ulman, S. Fanfan, A. Korniakov, and K. Loos. Mixed self-assembled monolayers of alkanethiolates on ultrasmooth gold do not exhibit contact-angle hysteresis. *Journal of the American Chemical Society*, 127(1):4–5, 2005. ISSN 0002-7863. doi: 10.1021/ja044623e. URL <GotoISI>://WOS:000226240900001.

[57] C. D. Bain and G. M. Whitesides. Molecular-level control over surface order in self-assembled monolayer films of thiols on gold. *Science*, 240(4848):62–63, 1988. ISSN 0036-8075. doi: DOI10.1126/science.240.4848.62. URL <GotoISI>://WOS:A1988M727800033.

[58] H. A. Biebuyck, C. D. Bian, and G. M. Whitesides. Comparison of organic monolayers on polycrystalline gold spontaneously assembled from solutions containing dialkyl disulfides or alkenethiols. *Langmuir*, 10(6):1825–1831, 1994. ISSN 0743-7463. doi: DOI10.1021/la00018a034. URL <GotoISI>://WOS:A1994NT58000034.

[59] K. L. Prime and G. M. Whitesides. Self-assembled organic monolayers - model systems for studying adsorption of proteins at surfaces. *Science*, 252(5009):1164–1167, 1991. ISSN 0036-8075. doi: DOI10.1126/science.252.5009.1164. URL <GotoISI>://WOS:A1991FN05600048.

[60] N. J. Geddes, E. M. Paschinger, D. N. Furlong, F. Caruso, C. L. Hoffmann, and J. F. Rabolt. Surface chemical activation of quartz-crystal microbalance gold electrodes - analysis by frequency changes, contact-angle measurements and grazing angle ftir. *Thin Solid Films*, 260(2):192–199, 1995. ISSN 0040-6090. doi: Doi10.1016/0040-6090(94)06474-1. URL <GotoISI>://WOS:A1995RA21400010.

[61] F. Jernstrom. *Self-assembled monolayers of alkanethiols: A study of surface composition, wettability, and adsorption of proteins and peptides.* Master thesis, 2001.

[62] K. Raiber, A. Terfort, C. Benndorf, N. Krings, and H. H. Strehblow. Removal of self-assembled monolayers of alkanethiolates on gold by plasma cleaning. *Surface Science*, 595 (1-3):56–63, 2005. ISSN 0039-6028. doi: 10.1016/j.susc.2005.07.038. URL <GotoISI>://WOS:000233315900009.

[63] Y. Cha, N. Matsuno, N. J. Rokainen-Matsuno, K. Jensen, and J. Gutow. Comparison of plasma and piranha cleaning for surface preparation of gold (au) prior to alkane thiol monolayer deposition using grazing incidence ir spectroscopy and microscopy. Report, Department of Chemistry, University of Wisconsin Oshkosh.

[64] S. M. Losslein, F. Mucklich, and P. G. Grutzmacher. Topography versus chemistry - how can we control surface wetting? *Journal of Colloid and Interface Science*, 609:645–656, 2022. ISSN 0021-9797. doi: 10.1016/j.jcis.2021.11.071. URL <GotoISI>://WOS:000772298700003.

[65] Biolin Scientific. Influence of droplet volume on contact angle. 2016.

[66] P. Jasrotia, B. Priya, R. Kumar, P. Bishnoi, A. Vij, and T. Kumar. A correlation between fractal growth, water contact angle, and sers intensity of r6g on ion beam nanostructured ultra-thin gold (au) films. *Frontiers in Physics*, 11, 2023. ISSN 2296-424x. doi: ARTN112500410.3389/fphy.2023.1125004. URL <GotoISI>://WOS:000959246100001.

[67] E. Ricci and R. Novakovic. Wetting and surface tension measurements on gold alloys. *Gold Bulletin*, 34(2):41–49, 2001. ISSN 0017-1557. doi: Doi10.1007/Bf03214811. URL <GotoISI>://WOS:000170886500002.

[68] J. Canning, N. Tzoumis, J. K. Beattie, B. C. Gibson, and E. Ilagan. Water on au sputtered films. *Chemical Communications*, 50(65):9172–9175, 2014. ISSN 1359-7345. doi: 10.1039/c4cc02492c. URL <GotoISI>://WOS:000339930400036.

[69] T. Smith. The hydrophilic nature of a clean gold surface. *Journal of Colloid and Interface Science*, 75(1):51–55, 1980. ISSN 0021-9797. doi: Doi10.1016/0021-9797(80)90348-3. URL <GotoISI>://WOS:A1980KB45000006.

[70] M. G. Paulik, P. A. Brooksby, A. D. Abell, and A. J. Downard. Grafting aryl diazonium cations to polycrystalline gold: Insights into film structure using gold oxide reduction, redox probe electrochemistry, and contact angle behavior. *Journal of Physical Chemistry C*, 111(21):7808–7815, 2007. ISSN 1932-7447. doi: 10.1021/jp0706578. URL <GotoISI>://WOS:000246695400036.

[71] F. Zina, N. M. Nooredeen, S. Azzouzi, M. Ben Ali, M. N. Abbas, and A. Errachid. Novel sensitive impedimetric microsensor for phosphate detection based on a novel copper phthalocyanine derivative. *Analytical Letters*, 51(3):371–386, 2018. ISSN 0003-2719. doi: 10.1080/00032719.2017.1322096. URL <GotoISI>://WOS:000418036900008.

[72] D. Yuan, K. Cadien, Q. Liu, and H. Zeng. *Impact of surface hydrophobicity and salinity on the adsorption of humic acids*. Thesis.

[73] J. Hedin, D. Isaksson, M. Andersson, and M. Nyden. Bi-layer formation of imidazole-modified ethyl(hydroxyethyl)cellulose at a hydrophobic surface as monitored by qcm-d. *Journal of Colloid and Interface Science*, 336(2):388–392, 2009. ISSN 0021-9797. doi: 10.1016/j.jcis.2009.04.033. URL <GotoISI>://WOS:000267671400002.

[74] Y. L. Ma, X. Y. Xiao, and Q. M. Ji. Design of surface nanostructures for chirality sensing based on quartz crystal microbalance. *Beilstein Journal of Nanotechnology*, 13: 1201–1219, 2022. ISSN 2190-4286. doi: 10.3762/bjnano.13.100. URL <GotoISI>://WOS:000879055800001.

[75] M. Edvardsson. What is the sauerbrey equation? 2020. URL https://www.biolinscientific.com/blog/what-is-the-sauerbrey-equation.

[76] M. Berglin and H. Elwing. Erosion of a model rosin-based marine antifouling paint binder as studied with quartz crystal microbalance with dissipation monitoring (qcm-d) and ellipsometry. *Progress in Organic Coatings*, 61(1):83–88, 2008. ISSN 0300-9440. doi: 10.1016/j.porgcoat.2007.09.010. URL <GotoISI>://WOS:000252941700012.

[77] Biolin Scientific. Qsense user guide: Instrument care and sensor pre-cleaning. .

[78] Qsense dfind.

[79] R. Sauter. Quality sensors. *Quantum Design*.

[80] Biolin Scientific. Overview: Characterization of polymer based systems. .

[81] P. Komorek, E. Martin, and B. Jachimska. Adsorption and conformation behavior of lysozyme on a gold surface determined by qcm-d, mp-spr, and ftir. *International Journal of Molecular Sciences*, 22(3), 2021. doi: ARTN132210.3390/ijms22031322. URL <GotoISI>://WOS:000615316800001.

A Appendices

A.1 Artificial Seawater Details

Lake Products Company LLC

PO Box 2658 Florissant, MO 63032 USA
www.lakeproductscompany.com
Tel: 314-770-2299 **sales@lakeproductscompany.com**

TECHNICAL BULLETIN
"SEA-SALT" ASTM D1141-98 (Re-approved 2013) Formula A, Table X1.1
Original Standard: ASTM D 1141-52, Formula A, Table 1, Section 4

DESCRIPTION: Sea-Salt is a simulated sea salt mix containing elements found in natural sea water in quantities greater than 0.0004%. Sea Salt is granular and colorless. Mixture contains U.S.P., N.F. and High-Grade Commercial Salts.

DIRECTIONS: Dissolve 41.953 grams Sea-Salt in water with enough water added to make one-liter total solution, or dissolve 5 ½ ounces (156 grams) Sea-Salt in water, then add enough water to make 1-gallon total solution of synthetic seawater. After mixing, adjust pH to 8.2 using 0.1 N solution of sodium hydroxide or hydrochloric acid. When mixing use Deionized (DI) or Distilled water for best results.

SPECIFICATIONS: Meets American Standard for Testing and Materials Standard D 1141-52, Formula a, Table 1, Section 4 and the updated Standard ASTM D 1141-98 (2013) Formula a, Table X1.1, Section 6 for duplicating ocean water.

COMPOSITION:

of Sea Salt mix	
NaCl	58.490%
$MgCl_2 \cdot 6H_2O$	26.460%
Na_2SO_4	9.750%
$CaCl_2$	2.765%
KCl	1.645%
$NaHCO_3$	0.477%
KBr	0.238%
H_3BO_3	0.071%
$SrCl_2 \cdot 6H_2O$	0.095%
NaF	0.007%

*Density of seawater equals 1.025 at 15°C
*Percentages of each component is measured by weight

of Substitute Ocean Water solution	
NaCl	24.53 g/L
$MgCl_2$	5.20 g/L
Na_2SO_4	4.09 g/L
$CaCl_2$	1.16 g/L
KCl	0.695 g/L
$NaHCO_3$	0.201 g/L
KBr	0.101 g/L
H_3BO_3	0.027 g/L
$SrCl_2$	0.025 g/L
NaF	0.003 g/L
Water	988.968 g/L
Total:	1025 g/L

APPLICATIONS: (Not intended for human consumption)

CORROSION STUDIES: Accelerated corrosion studies where effects of seawater on the following: Ferrous and non-ferrous metals, plastics, protective coatings, paint, electrochemical processes, surface active agents and ceramics.

BIOLOGICAL: Supports marine biological life. Can also be used as a tissue and muscle preservative.

CHEMICAL PROCESSING: Activity effects of minor trace elements may be compared in chemical processing units.

OCEAN INSTRUMENT TESTING: Standardizes seawater environment for consistent test comparisons.

Updated: 8/2021

A.2 Contact Angle on Polymer Surfaces

Table A.1: Contact angle on SAM of MUA

	Sensor 1	Sensor 2	Sensor 3	Sensor 4
Exp. 1	37.5 ± 0.6	43.8 ± 1.2	36.5 ± 0.4	37.0 ± 0.4
Exp. 2	41.8 ± 0.8	45.1 ± 0.7	42.5 ± 0.8	41.1 ± 0.8

Table A.2: Contact angle on SAM of MUOH

	Sensor 1	Sensor 2	Sensor 3	Sensor 4
Exp. 1	42.1 ± 1.0	48.1 ± 0.6	44.1 ± 1.0	45.3 ± 1.6
Exp. 2	39.3 ± 0.9	39.4 ± 1.7	36.0 ± 0.2	39.9 ± 0.9

Table A.3: Contact angle on SAM of DT10

	Sensor 1	Sensor 2	Sensor 3	Sensor 4
Exp. 1	105.1 ± 0.2	104.8 ± 0.6	105.7 ± 1.7	105.2 ± 0.4
Exp. 2	103.3 ± 0.9	103.2 ± 0.6	104.7 ± 1.6	102.6 ± 1.0

Table A.4: Contact angle on SAM of AUT

	Sensor 1	Sensor 2	Sensor 3	Sensor 4
Exp. 1	54,3 ± 1.6	54.8 ± 0.8	54.0 ± 1.7	54.7 ± 1.3
Exp. 2	56.0 ± 1.4	55.8 ± 0.5	56.8 ± 1.8	56.7 ± 0.5

A.3 Model Fit Values

Table A.5: Fit values for model used in the different experiments.

	MUA	MUOH	DT10	AUT
Lys	0.74	0.63	0.7	0.74
BSA	0.96	0.98	0.95	0.93
Lys/BSA	0.96	0.78	0.96	0.77
Sequential deposition	0.88	0.75	0.87	0.78

A.4 ΔD/ΔF Plots for all Polymers

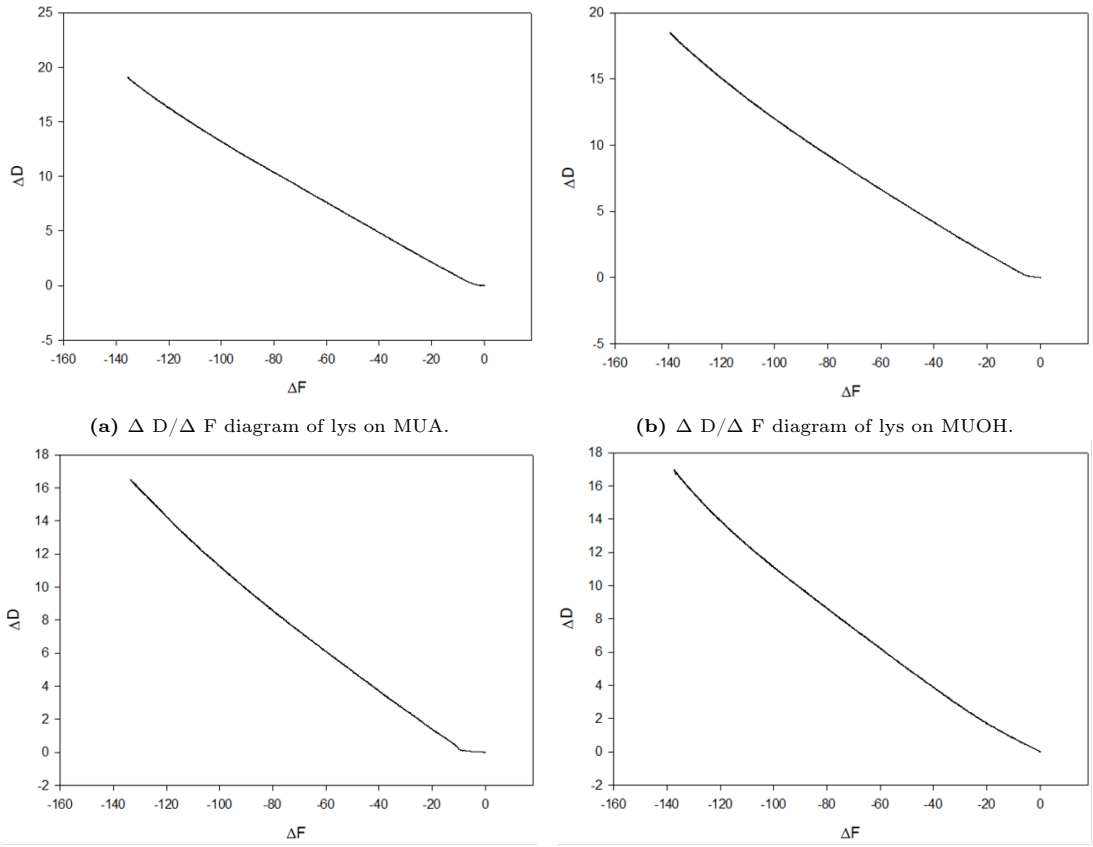

(a) Δ D/Δ F diagram of lys on MUA.

(b) Δ D/Δ F diagram of lys on MUOH.

(c) Δ D/Δ F diagram of lys on DT10.

(d) Δ D/Δ F diagram of lys on AUT.

Figure A.1: Layer softness per mass during lysozyme adsorption on the four SAM surfaces.

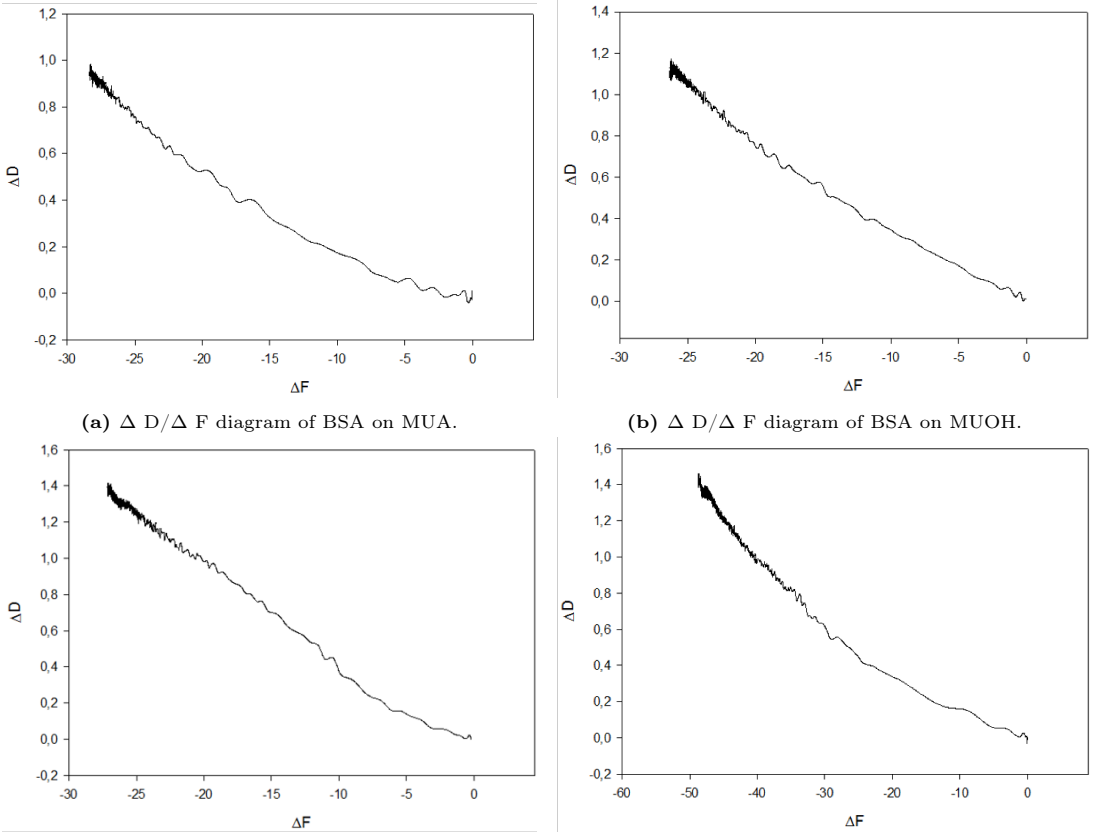

(a) Δ D/Δ F diagram of BSA on MUA.

(b) Δ D/Δ F diagram of BSA on MUOH.

(c) Δ D/Δ F diagram of BSA on DT10.

(d) Δ D/Δ F diagram of BSA on AUT.

Figure A.2: Layer softness per mass during BSA adsorption on the four SAM surfaces.

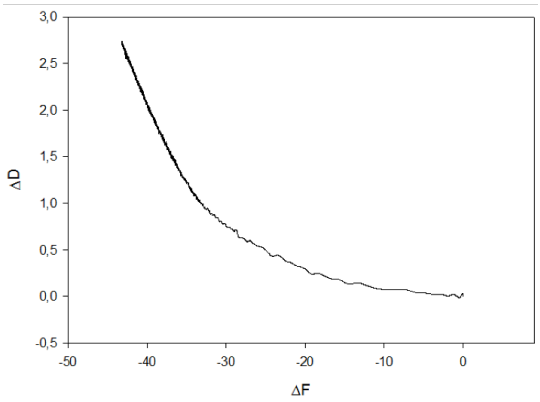

(a) Δ D/Δ F diagram of lys/BSA on MUA.

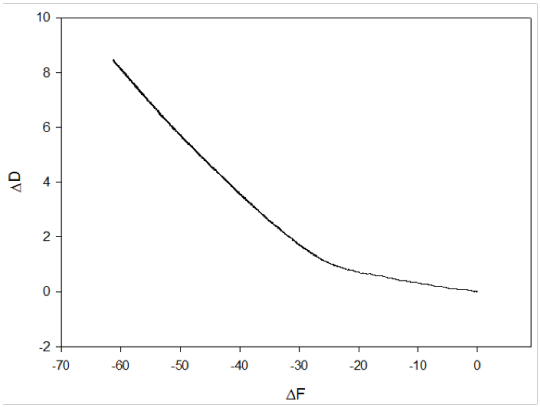

(b) Δ D/Δ F diagram of lys/BSA on MUOH.

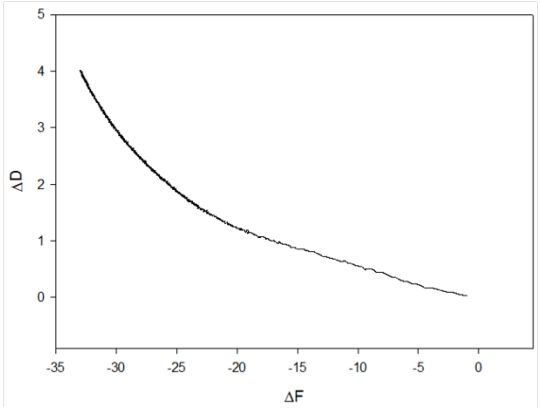

(c) Δ D/Δ F diagram of lys/BSA on DT10.

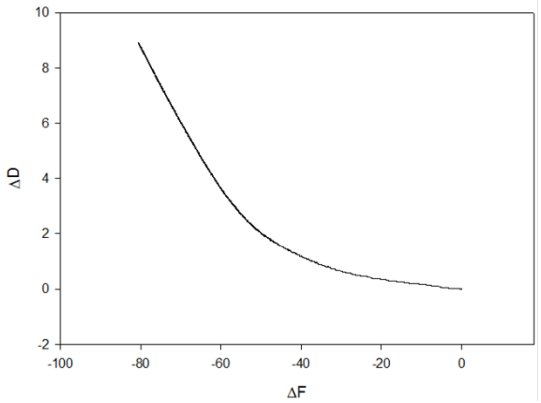

(d) Δ D/Δ F diagram of lys/BSA on AUT.

Figure A.3: Layer softness per mass during lysozyme/BSA adsorption on the four SAM surfaces.

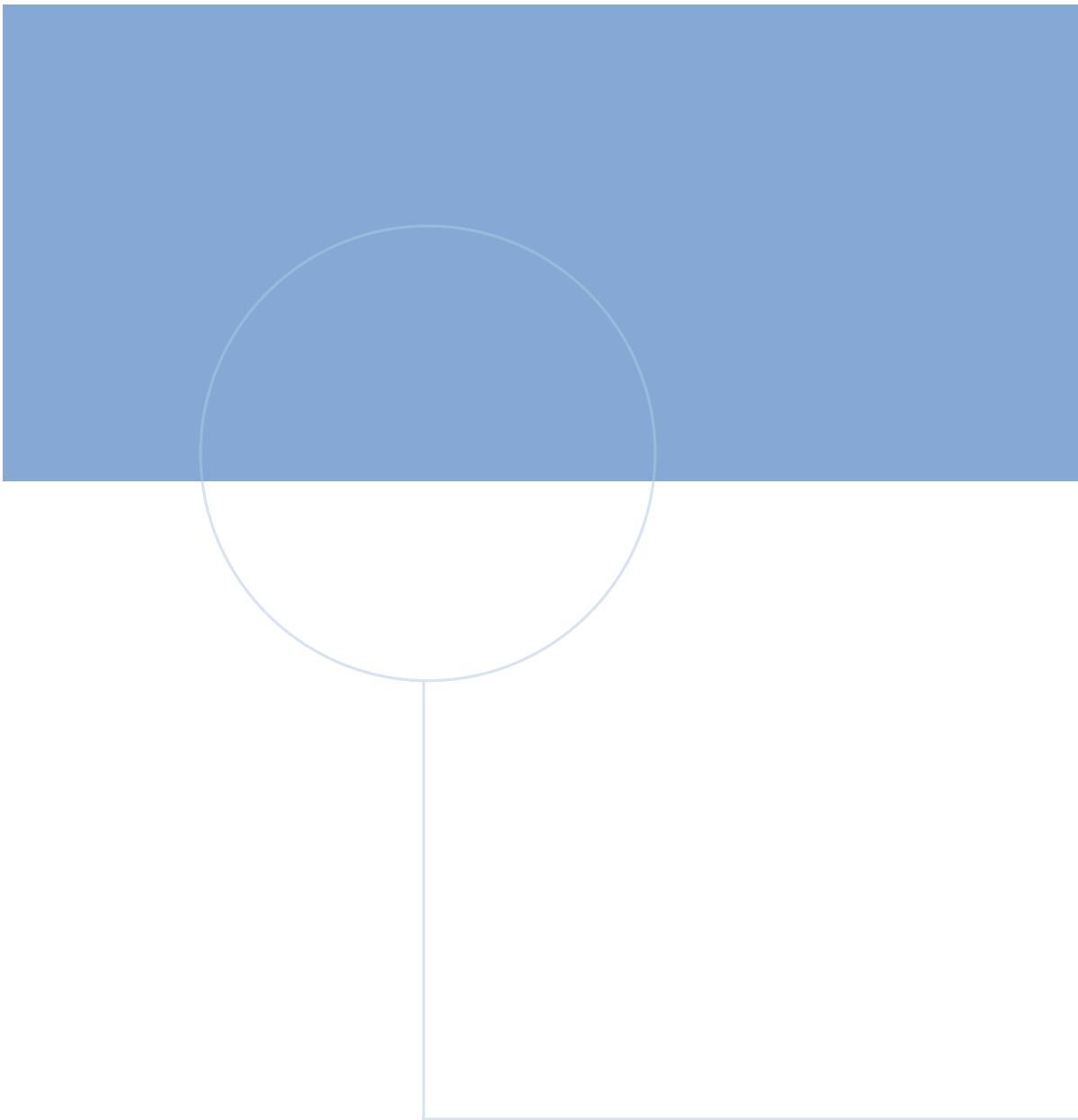

NTNU

Norwegian University of
Science and Technology